

PAPER • OPEN ACCESS

Semiconductor/lithium lanthanum titanate perovskite interface: a DFT study

To cite this article: J M Cervantes *et al* 2025 *Phys. Scr.* **100** 035971

View the [article online](#) for updates and enhancements.

You may also like

- [\(Digital Presentation\) Negative Bias Illumination Stress on a-lgzo TFT with a Top Barrier](#)
Jih-Chao Chiu, Eknath Sarkar, Yuan-Ming Liu et al.
- [Enhanced Stability Under Positive Bias Temperature Stress in Oxide Thin Film Transistors with Double Gate Structure By Improving Bottom Channel Interface](#)
Kyoung-Seok Son, Myoeng-Ho Kim, Seung-Hun Lee et al.
- [Adjustable Silicon Corner Rounding Radius by Wet Technique](#)
Pei-Ting Tou, Hsin-Yi Liao, Hui-Chin Huang et al.



OPEN ACCESS

PAPER

Semiconductor/lithium lanthanum titanate perovskite interface: a DFT study

RECEIVED

11 June 2024

REVISED

25 January 2025

ACCEPTED FOR PUBLICATION

14 February 2025

PUBLISHED

25 February 2025

J M Cervantes¹ , J E Antonio² , H Muñoz¹ , R O Escamilla³ , M Romero² and R Escamilla¹ ¹ Instituto de Investigaciones en Materiales, Universidad Nacional Autónoma de México. A.P. 70-360, Ciudad de México, 04510, Mexico² Facultad de Ciencias, Universidad Nacional Autónoma de México. A.P. 70-399, 04510, Ciudad de México, Mexico³ Escuela Superior de Ingeniería Mecánica y Eléctrica-Culhuacán, Instituto Politécnico Nacional, Av. Santa Ana 1000, Ciudad de México, 04440, MexicoE-mail: josemiguel.cervantes.gin2013@gmail.com, jaime.antonio.gin2017@gmail.com and rauleg@unam.mx**Keywords:** semiconductor/oxide interface, magnetic properties, nanostructured systems, perovskites

Original content from this work may be used under the terms of the Creative Commons Attribution 4.0 licence.

Any further distribution of this work must maintain attribution to the author(s) and the title of the work, journal citation and DOI.

**Abstract**

Currently, incorporating functional materials such as Si and Ge semiconductors on perovskite-type oxide titanates is essential to exploit their electronic and magnetic properties. In this work, the electronic and magnetic properties of Si/Ge monolayer (ML) on a LaO-terminated LaTiO_3 (LTO) or LiO-terminated $\text{Li}_{0.5}\text{La}_{0.5}\text{TiO}_3$ (LLTO) surface, at La-, O- and Li-top sites systems were studied through the Density Functional Theory. Our results show that the system has an antiferromagnetic order when the Si-ML is on the O-top site of the LTO surface; and ferromagnetic when the Si-ML is on the O-top site of the LLTO surface. All the remaining Si adsorption cases are ferrimagnetic systems. When the Ge ML is placed at the La-top and O-top sites on the LTO surface, the resulting systems exhibit ferrimagnetism. In contrast, the Ge-ML on the LLTO surface shows ferromagnetism, regardless of the adsorption site. The adsorption energy values show that the most favorable site to place the Si/Ge ML on the LLTO perovskite surface is at the O-top site. These results display that Si/Ge semiconductor ML/oxide perovskite surface could be used as interface in electrochemical systems.

Introduction

The electronic and magnetic properties of perovskite-type oxides have attracted attention because these materials present ferroelectricity, ferromagnetism and superconductivity [1]. However, inducing substitution defects, quantum confinement or the integration of functional oxides open new fields of application in devices with improved functionalities [2]. Developments in experimental techniques, such as molecular beam epitaxy (MBE) and pulsed laser deposition (PLD), have made possible the epitaxial and coherent growth of oxide films with abrupt interfaces [3, 4]. Unfortunately, it is difficult to predict the atomic structure and composition of heterostructures as they grow. Hence, it is important to predict the physical properties of the composition and structure of the semiconductor/oxide surface and interface. In recent years, there has been significant attention in studying hybrid materials composed of ABO_3 perovskite-type oxides and semiconductor materials with a zinc-blende or diamond structure. This is because the epitaxial growth of single crystal perovskites on semiconductor substrates with limited structural defects at the semiconductor/oxide interface make them excellent structures for the integration into photovoltaic, electrochemical, magnetic, ferroelectric or piezoelectric devices [5]. For example, the epitaxial growth of perovskite oxides on Si [6–12] and Ge [13–16].

Experimental and theoretical results have shown that the growth of SrTiO_3 (STO) on silicon prevents insulating states and induces ferroelectricity through epitaxial tension. These results indicate that heterostructures with a semiconductor/oxide interface can be used in tunnel junctions and in ferroelectric field effect transistors (FEFET) [17–19]. The development of STO induced the study of new materials with heterojunctions, such as PbTiO_3 (PTO), BaTiO_3 (BTO) and LaAlO_3 (LAO) on a Si/Ge semiconductor substrate [15, 20–22]. In the electro-optical field, BTO is an ideal material for the development of modulators and light wave circuit elements. The interface exhibits a polarization caused by the difference in thermal expansion

coefficients between the slab and the substrate [23–25]. Particularly, to grow LaTiO_3 (LTO) perovskite on Si or Ge, an intermediate STO layer is required [26]. This material has been very interesting, since the LTO/STO interface is formed by an LTO thin layer that is grown epitaxially on the STO surface, and since the Ti atoms have an oxidation state of 3^+ and 4^+ in the LTO and STO perovskites, respectively, at the LTO/STO interface there is a two-dimensional high mobility of electrons [27].

Another way to modulate the properties of materials is through defects in their structure. One way to achieve this is through solid solutions. This can be observed by alloying the B-site Ti cations with Zr, forming $\text{SrTi}_{1-x}\text{Zr}_x\text{O}_3$ where the increase of Zr in STO increases the conduction band of the oxide above the Ge conduction band and consequently, the formation of a barrier of electron transport [28]. On the other hand, $\text{La}_{1-x}\text{Sr}_x\text{MnO}_3$ (LSMO) in a composition close to $x = 0.33$, exhibits a transition from insulator to metal as the temperature decreases. This behavior could be used in micro-electromechanical systems (MEMS) devices [29]. Likewise, LSMO exhibits a high spin polarization, this is ideal in the integration of semiconductors used in spintronics and optospintrronics [30]. In this sense, when substitutional Li-defects are incorporated into the LTO perovskite, different phases of $\text{Li}_x\text{La}_{1-x}\text{TiO}_3$ bulk perovskites (LLTO) can be obtained depending on the Li concentration and the Li-hosting sites, generating suitable materials for Li-ion battery development [31]. Thus, the LLTO perovskite is a good candidate to be used as a solid electrolyte, since, the ions' mobility could be through the structure's vacancies, which allows the ionic conductivity to be closer to that of liquid electrolytes [32, 33]. Recently, the synthesis of LLTO perovskite on a semiconductor material was achieved [34].

Although semiconductor/oxide materials on semiconductor substrates have been widely explored, there are few studies considering these oxides as a substrate. Experimental studies on Ge in STO [35–37] as well as Si and Ge in LAO [38] indicate that the (001) and (111) growth of semiconductors is modulated by the temperature of the (001) oxide substrate. Theoretical studies about Ge on STO [39, 40], SrHfO_3 [41] and SrZrO_3 [42] describe a metallic surface, where the semiconductor/oxide interface can facilitate the performance of metal-oxide semiconductor field-effect transistors and monolithically integrated optoelectronics devices. In the case of the structural and electronic compatibility between Si and Ge bulk materials on LTO or LLTO surfaces has not yet been explored. Motivated by this background, this work seeks to expand the research as well as to understand how to control the electronic and magnetic properties of the interface between Si/Ge semiconductor monolayer and LTO/LLTO perovskite surface.

Computational methodology and atomistic models

The ground state and physical properties of the interface between Si/Ge semiconductor and LTO/LLTO perovskite have been determined using Density Functional Theory (DFT) as implemented in the CASTEP code [43]. Standard norm-conserving pseudopotentials were used [44], therefore, the valence electrons $2s^1$ for Li, $5d^16s^2$ for La, $3s^2p^64s^23d^2$ for Ti and $2s^2p^4$ for O were contemplated. A cut off energy of 500 eV was used. To take into account the electron correlation effects of the Ti-*d* orbitals and have a good description of the electronic and magnetic properties of LTO/LLTO perovskite, all calculations were performed with the Hubbard-corrected Local Density Approximation (LDA+U, $U_{\text{Ti-}d} = 2.50$ eV) [45], with the exchange–correlation Ceperley and Alder functional, parameterized by Perdew and Zunger (CA-PZ) [46, 47]. The chosen $U_{\text{Ti-}d}$ value was taken from [48]. As will be described in detail below, the electronic energy band gap and the magnetic moment of Ti atoms determined with a $U_{\text{Ti-}d} = 2.50$ eV agree well with the experimental values. The Brillouin zone was sampled using a $4 \times 4 \times 1$ grid on the Monkhorst–Pack scheme [49]. To determine the total energy of ground state of the physical system, the convergence was reached when the energy difference between the last two steps of the self-consistent field (SCF) process was less than 2.00×10^{-5} eV atom $^{-1}$. For structural relaxation, the two-point steepest descent method (TPSD) was used [50]. All the atoms were fully relaxed until the residual forces on each atom were converged to 0.05 eV Å. Likewise, during the geometric optimization, the convergence parameters used were 2.00×10^{-5} eV atom $^{-1}$ for maximum energy change, 0.10 GPa for the maximum external stress applied, and 2.00×10^{-3} Å for the maximum atomic displacement.

To build the semiconductor/oxide interface models we used the following procedure: from the experimental room-temperature orthorhombic crystalline structure relaxed of LTO perovskite [51], a two-dimensional (2D) nanostructure was constructed, by exposing free surfaces parallel to the (001) crystalline plane, with LaO termination. The motivation for modeling the surfaces by exposing (001) atomic planes is that there are many experimental methods with established success in synthesizing thin films of ABO_3 perovskite-type materials. These methods involve exposing the AO or BO_2 terminations parallel to the (001) crystalline planes [20, 30, 35, 37, 52–54]. On the other hand, based on the ionic model, to maintain electroneutrality in the LLTO bulk perovskite, the anions and cations of Li, La, Ti, and O must exhibit oxidation states of 1+, 3+, 4+, and 2-, respectively [55]. To satisfy this condition, the concentration of substitutional Li must be $x = 0.50$. If La is substituted by Li in the LTO perovskite with a concentration of 0.50, three possible structural phases (layered,

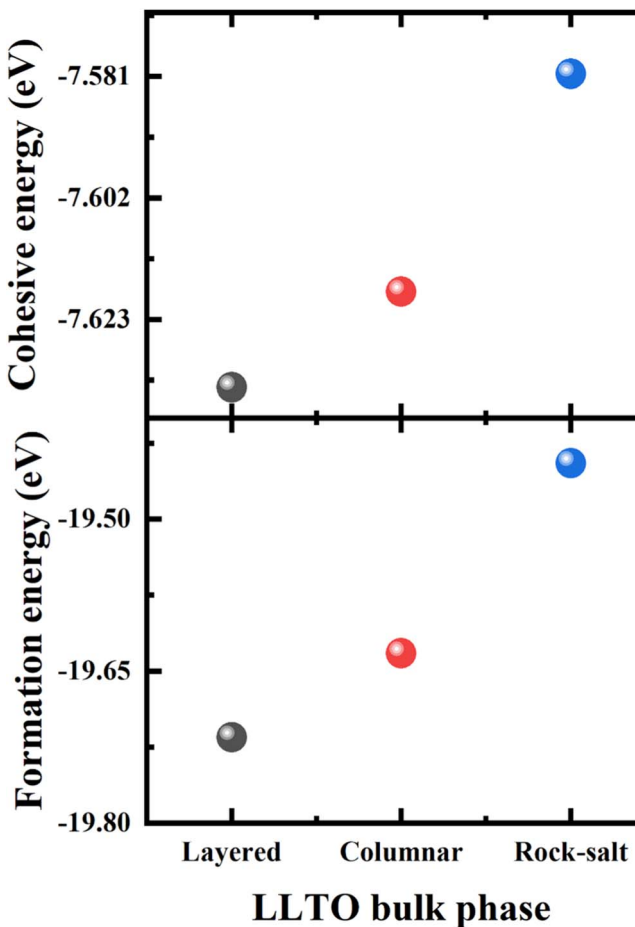


Figure 1. Cohesive and formation energies of LLTO-layered, -columnar and -rock-salt bulk phases.

columnar, and rock-salt) can be formed. These LLTO structural bulk phases depend on the Li location and are detailed in [55–59]. To determine the most stable structural phase, we conducted calculations of the cohesive and formation energies of these LLTO compounds (figure 1). The cohesive energy was calculated using the following expression [56],

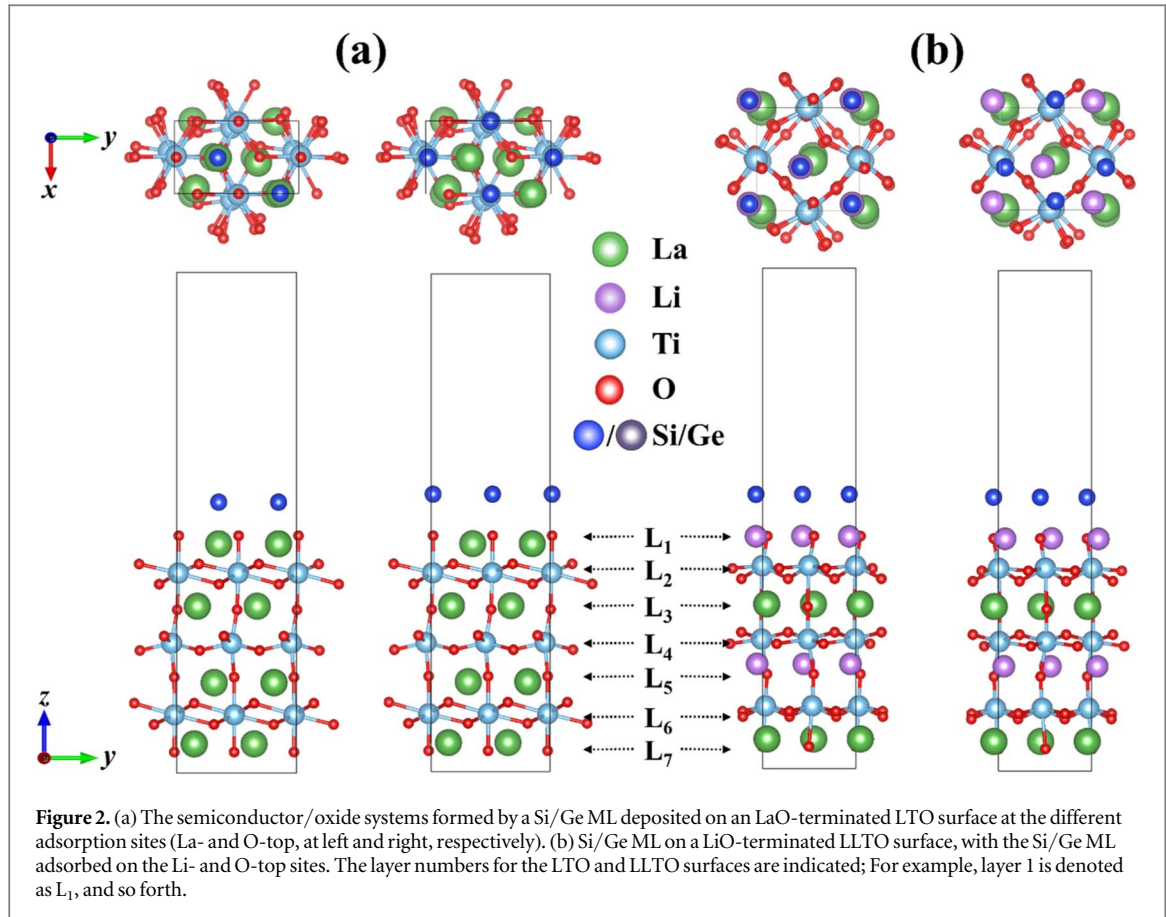
$$E_{cohesive} = \frac{E_{bulk} - \sum_i n_i E_i}{N}. \quad (1)$$

E_{bulk} is the energy of LLTO bulk phase. n_i and E_i represent the number of species i in the LLTO compound and the energy of the isolated atom i , respectively. N is the total number of atoms in the unit cell. The formation energy of the LLTO bulk phases (E_{form}^{LLTO}) was computed by using the equation below [55]:

$$E_{form}^{LLTO} = E_{LLTO} - 0.5 \mu_{\text{Li}} - 0.5 \mu_{\text{La}} - \mu_{\text{Ti}} - \frac{3}{2} \mu_{\text{O}_2}. \quad (2)$$

E_{LLTO} represented the total energy of the LLTO stoichiometric unit. μ_{Li} , μ_{La} , μ_{Ti} and μ_{O_2} are the chemical potentials of the Li, La, Ti and a O_2 molecule, respectively. For the calculation of chemical potentials, a body-centered cubic structure was used as the reference phase for Li, whereas a hexagonal close-packed structural phase was used for La and Ti. The chemical potentials of lithium, lanthanum, and titanium are defined as the energy of the reference structural bulk phases per atom. In the μ_{O_2} case, the chemical potential represents the energy of an O_2 molecule in a cubic unit cell with dimensions of 10 Å. This unit cell is used to avoid interactions between periodic images.

The results indicate that the LLTO layered structural phase is the most stable, followed by the columnar and rock-salt phases. These findings are in line with previous research [55–59]. Furthermore, this structural phase is consistent with experimental observations, where the Li atoms are positioned in layered sites within the LLTO compound [31, 32, 60, 61]. Consequently, another 2D nanostructure was constructed: First substituting La by Li atoms, to generate the $\text{Li}_{0.5}\text{La}_{0.5}\text{TO}_3$ (LLTO) layered perovskite, from which was cut a slab with exposed (001) LiO -terminated surface. In these LaO -terminated LTO and LiO -terminated LLTO surface models, the metal atom at the surface changes its coordination number from 12 to 8 oxygens. Likewise, the coordination number



of the oxygen atoms at the surface is modified from 6 to 5; The oxygen is surrounded by four La/Li atoms and a Ti atom.

Once the LTO and LLTO surfaces were built, the most favorable site to place a Si or Ge monolayer (ML) on these surfaces was determined; Then the Si or Ge ML was placed on the LaO-terminated LTO or LiO-terminated LLTO surfaces at the La-, O- and Li-top adsorption sites, the coverage of Si/Ge was 1/2 ML (figure 2). A vacuum of 15 Å was left along the z-direction to avoid interactions between semiconductor/oxide systems. It is important to note that we have limited the LTO/LLTO surface thickness to 7 layers due to computational cost. We assume that the Si/Ge ML will interact with the first 3 layers of the LaO-terminated LTO and LiO-terminated LLTO surfaces. Therefore, this thickness is sufficient to study this interaction. Consequently, we employed antisymmetric adsorption models and then freely optimized the atomic positions (figure 2). However, the surface reconstruction of the inferior layers of the LaO-terminated LTO and LiO-terminated LLTO surfaces could impact the charge redistribution in the central layers and potentially influence the electronic states at the Fermi level (E_F) [62]; Thus, these effects are also studied.

To quantify the structural deformations of LTO and LLTO surfaces after the adsorption of Si or Ge ML, we measured and compared the interplanar distances of the surfaces for each adsorption case with those of the pristine surface and the bulk phase. The interplanar distances were calculated using the following expression:

$$d_{i,i+1} = z_{i+1} - z_i, \quad (3)$$

where z_i (z_{i+1}) is the average z-coordinate of the atoms of layer i ($i + 1$). The change in the interplanar distances with respect to those presented in the bulk phase is measured with the $\delta_{i,i+1}$ parameter,

$$\delta_{i,i+1} = \frac{d_{i,i+1} - d_0}{c_0} \times 100\%, \quad (4)$$

where d_0 is the interplanar distance in the LTO or LLTO bulk and c_0 is the theoretical value of lattice parameter c of LTO (or LLTO) bulk phase. To measure the distance between the Si/Ge ML and the LaO (or LiO)-terminated LTO (or LLTO) surface, the equilibrium distance (Δd) was calculated. Δd was computed as follows:

$$\Delta d = w_i - w_{\text{average}}, \quad (5)$$

where w_i represent the z-coordinate of i atom closest to the first layer of the LTO or LLTO surface (with $i = \text{Si}$ or Ge). w_{average} denotes the average z-coordinate of atoms at the layer 1.

Table 1. Structural parameters of LTO bulk phase (in Å): lattice parameters a , b , and c , as well as the Ti-O and O-O equatorial bond lengths ($d_{1(\text{Ti}-\text{O})}$, $d_{2(\text{Ti}-\text{O})}$, $d_{1(\text{O}-\text{O})}$, and $d_{2(\text{O}-\text{O})}$). Besides, the magnitude of magnetic moment of Ti atoms (μ , in μ_B) and the energy band gap (E_g in eV).

References	Approximation	MC	a	b	c	$d_{1(\text{Ti}-\text{O})}$	$d_{2(\text{Ti}-\text{O})}$	$d_{1(\text{O}-\text{O})}$	$d_{2(\text{O}-\text{O})}$	μ	E_g
This work	DFT-LDA + U	AFM _G	5.15	5.70	7.32	1.99	2.04	2.77	2.92	0.58	0.47
Komarek <i>et al</i> [51]	Experimental	AFM _G	5.64	5.62	7.92	2.03	2.06	2.94	2.85	—	—
Okimoto <i>et al</i> [64]	Experimental	—	—	—	—	—	—	—	—	—	0.20
Cwik <i>et al</i> [65]	Experimental	AFM _G	—	—	—	—	—	—	—	0.57	—
Goral <i>et al</i> [66]	Experimental	AFM _G	—	—	—	—	—	—	—	0.45	—
El-Mellouhi <i>et al</i> [67]	DFT-HSE06	AFM _G	5.60	5.53	7.90	—	—	—	—	0.94	1.27
Streltsov <i>et al</i> [48]	LMTO-LDA + U	AFM _G	—	—	—	—	—	—	—	0.78	0.57
Gu <i>et al</i> [68]	DFT-GGA + U	AFM _G	5.65	5.67	7.92	—	—	—	—	—	1.89
Filippetti <i>et al</i> [69]	DFT-VPSIC	AFM _G	—	—	—	—	—	—	—	0.89	1.60

To analyze the electronic charge redistributions between the Si/Ge ML and the LTO or LLTO surface, the Hirshfeld analysis and the electronic density difference (EDD) were obtained. EDD was calculated using the equation:

$$\Delta\rho = \rho_{\text{Si (Ge) ML/LTO (LLTO) surface}} - \rho_{\text{LTO (LLTO) surface}} - \rho_{\text{Si (Ge) ML}}, \quad (6)$$

where $\rho_{\text{Si (Ge) ML/LTO (LLTO) surface}}$ is the electronic density of the semiconducting oxide systems.

$\rho_{\text{LTO (LLTO) surface}}$ and $\rho_{\text{Si (Ge) ML}}$ are the electronic densities of the LTO (LLTO) surface and the isolated Si/Ge ML, respectively.

Likewise, the adsorption energies (E_{ads}) were calculated using the equation:

$$E_{ads} = (E_{\text{Si (Ge) ML/LTO (LLTO) surface}} - E_{\text{LTO (LLTO) surface}} - nE_{\text{Si (Ge)}})/n. \quad (7)$$

Where $E_{\text{Si (Ge) ML/LTO (LLTO) surface}}$ and $E_{\text{LTO (LLTO) surface}}$ are the total energy of Si/Ge ML on the LTO (LLTO) surface, and pristine LTO (LLTO) surface, respectively. n and $E_{\text{Si (Ge)}}$ are the number and the energy of the Si/Ge atoms. The negative E_{ads} denotes an exothermic adsorption process. Since interactions of the van der Waals type can exist between the Si/Ge ML and the LTO/LLTO surface, the semi-empirical van der Waals correction proposed by Ortmann *et al* [63] was used to calculate E_{ads} . In this approximation, the energy corresponding to the long-range electronic correlation interactions is added to the total DFT energy, which is defined as follows,

$$E^{\text{vdW}} = -\frac{1}{2}\sum_{i,j} f_{ij}(R)\frac{C_6^{ij}}{R^6}, \quad (8)$$

where $f_{ij}(R)$ is the damping function. R is the distance at which the pair of interacting atoms i and j are separated. In this approximation, $f_{ij}(R)$ is modeled as a function with exponential decay and has the form $f_{ij}(R) = 1 - e^{-\lambda x_{ij}^n}$. x_{ij}^n is the normalized R value with respect to the sum of the covalent radii r_{cov}^i y r_{cov}^j of two interacting atoms, i.e. $x_{ij}^n = R/(r_{\text{cov}}^i + r_{\text{cov}}^j)$. $C_6^{ij} = \frac{3}{2}\alpha_i\alpha_j\frac{I_i I_j}{I_i + I_j}$, where I_i is the ionization potential and α_i is the polarizability of the atom i .

Results and discussion

The methodology is validated by comparing the structural, electronic and magnetic properties of the LTO bulk perovskite with the available experimental and theoretical studies (table 1). A G-type antiferromagnetic configuration (AFM_G) was modeled for the LTO. The formal spin of the Ti atoms was aligned antiparallel along the [110], [1 $\bar{1}$ 0] and [001] directions (figure 3(a)). Once the ground state was identified, the structural parameters were compared with those reported from experimental work (table 1). The results show that the lattice parameters a , b and c as well as the Ti-O and O-O equatorial bond lengths agree with the experimental data. Similarly, the size of the indirect energy band gap (E_g) is 0.47 eV. The valence band maximum (VBM) and conduction band minimum (CBM) are located at the high symmetry points T and Γ (figure 3(b)). Besides, the E_g value found is close to that reported experimentally (table 1). Likewise, the distribution of magnetic moments (μ) of Ti atoms converged to AFM_G with a magnitude of $0.58\ \mu_B$, which is consistent with experimental and theoretical observations (table 1).

Furthermore, PDOS analysis reveals that the main contribution to the valence and conduction bands at the E_F comes from the Ti-*d* orbitals, followed by contributions from the O-*p* and La-*d* orbitals (figure 3(b)). These findings are consistent with other theoretical studies [48, 67–69]. Likewise, the presence of La³⁺, Ti³⁺, and O²⁻ ions is qualitatively confirmed by the Hirshfeld charges. The ratios between La:O and Ti:O charges are 1.38 and 1.65, respectively, they are close to the ideal value of 1.5 (table 2). Once the LTO perovskite structure

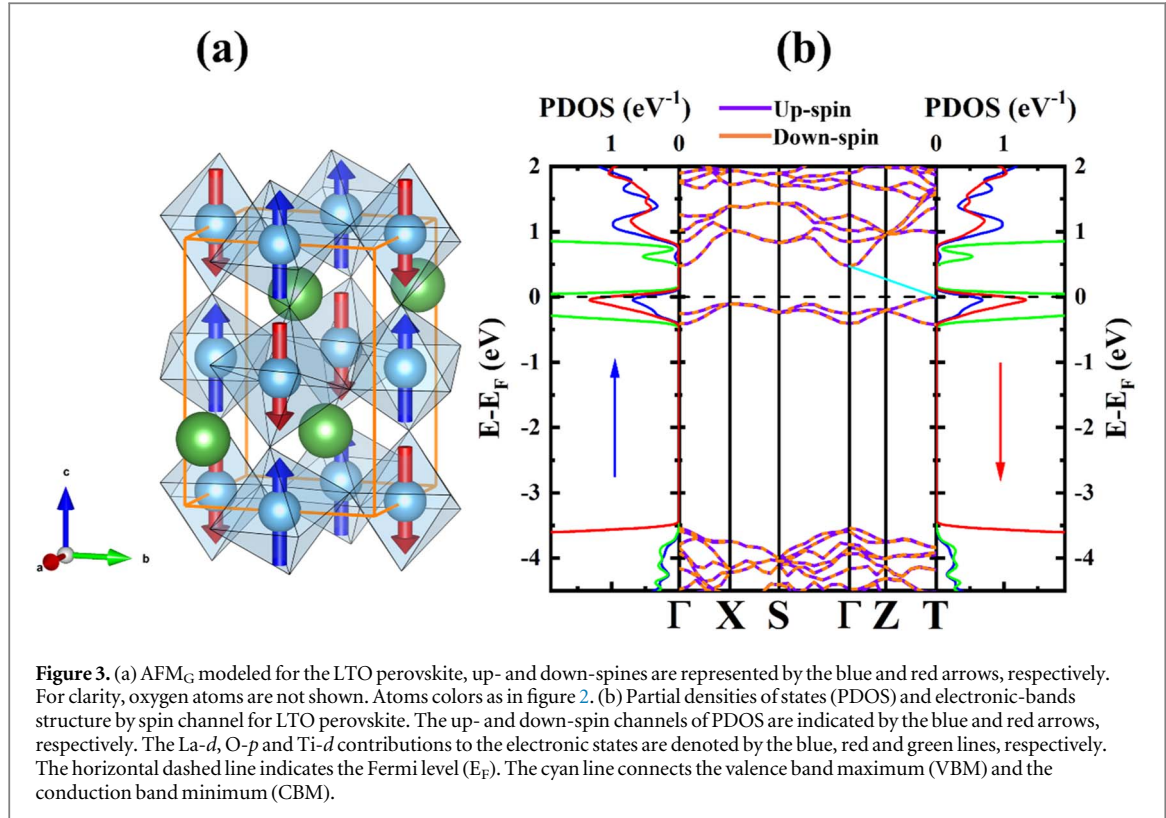


Figure 3. (a) AFM_G modeled for the LTO perovskite, up- and down-spins are represented by the blue and red arrows, respectively. For clarity, oxygen atoms are not shown. Atoms colors as in figure 2. (b) Partial densities of states (PDOS) and electronic-bands structure by spin channel for LTO perovskite. The up- and down-spin channels of PDOS are indicated by the blue and red arrows, respectively. The La-*d*, O-*p* and Ti-*d* contributions to the electronic states are denoted by the blue, red and green lines, respectively. The horizontal dashed line indicates the Fermi level (E_F). The cyan line connects the valence band maximum (VBM) and the conduction band minimum (CBM).

Table 2. Electronic charges (in e units) of Ti, La, O, and Li ions for LTO and LLTO bulk phases.

LTO			LLTO			
Ti	La	O	Ti	La	Li	O
0.48	0.40	-0.29	0.63	0.36	0.17	-0.30

incorporates Li atoms, Ti^{3+} cations lose electronic charge, resulting in the conversion from Ti^{3+} to Ti^{4+} cations as qualitatively is noted by the electronic charges of LLTO bulk phase (table 2).

Once the methodology was validated, eight semiconductor/oxide interface systems formed by a Si or Ge ML at the different adsorption sites (La-, Li- and O-top) on an LTO or LLTO surface were studied (figure 2). These systems are designated as *A* ML/C surface, where *A* is the chemical composition of the ML (Si or Ge), and C designates the substrate (LTO or LLTO). When the Si/Ge ML is adsorbed on the LaO-terminated LTO surface at the La-top site, the Si/Ge atoms shift away from the La atoms in the substrate layer. This movement results in the formation of zigzag-shaped atomic chains of Si/Ge that grow periodically along the [001] direction (figures 5 and 6). When the Si or Ge ML is positioned at the Li-top site on the LiO-terminated LLTO substrate, Si/Ge atoms shift toward the O-top adsorption sites (figures 5 and 6). Likewise, the Si or Ge atoms do not move significantly when adsorbed at the O-top sites of the LTO and LLTO surfaces (figures 5 and 6).

The effect of Si/Ge adsorption on LTO and LLTO surfaces due to structural relaxation is evaluated by comparing the interplanar distances of the Si (or Ge)/LTO (or LLTO) surface systems with those of the bulk and LTO and LLTO surfaces before adsorption (table 3). For the LTO pristine surface, all interplanar distances decrease, with the most notable contractions occurring in $d_{1,2}$ and $d_{6,7}$, which decrease by 1.67% and 1.66%, respectively. In contrast, the LLTO pristine surface shows increases in $d_{1,2}$, $d_{3,2}$, and $d_{5,6}$, while $d_{3,4}$, $d_{4,5}$, and $d_{6,7}$ decrease. The largest increase is observed on $d_{5,6}$, which increases by 4.28%, whereas the greatest contraction is observed in $d_{4,5}$, which decreases by 2.09%.

Besides, by comparing the interplanar distances and their corresponding changes for the LTO and LLTO pristine surfaces with those observed in the Si (or Ge)/ LTO (or LLTO) surface systems, it is possible to conclude that structural relaxation caused by Si/Ge adsorption affects not just the first layers of the LTO and LLTO surfaces, but also causes interplanar displacements in the lower layers (see table 3). For the Si (or Ge) ML/LTO surface cases, the surface reconstruction results in a decrease in all interplanar distances except for $d_{4,5}$. For these semiconductor/oxide interfaces, the changes in interplanar distances are similar. For instance, in the Si ML case,

Table 3. Interplanar distances ($d_{i,j}$, in Å) for LTO and LLTO bulk phases as well as for LTO and LLTO pristine surfaces and for the cases where the Si or Ge ML is adsorbed on LaO-terminated LTO or LiO-terminated LLTO surfaces. Likewise, the $\delta_{i,j}$ parameter (in %) and the distance between the Si/Ge ML and the LTO (or LLTO) surface (equilibrium distance Δd , in Å).

	$d_{1,2}$	$d_{2,3}$	$d_{3,4}$	$d_{4,5}$			
LTO bulk	1.86	1.86	1.86	1.86			
LLTO bulk	1.94	1.80	1.80	1.95			
LTO pristine surface	$d_{1,2} (\delta_{1,2})$ 1.73 (-1.67)	$d_{2,3} (\delta_{2,3})$ 1.83 (-0.35)	$d_{3,4} (\delta_{3,4})$ 1.83 (-0.39)	$d_{4,5} (\delta_{4,5})$ 1.84 (-0.27)	$d_{5,6} (\delta_{5,6})$ 1.84 (-0.25)	$d_{6,7} (\delta_{6,7})$ 1.73 (-1.66)	
LLTO pristine surface	1.99 (0.57)	1.84 (0.54)	1.80 (-0.03)	1.79 (-2.09)	2.26 (4.28)	1.72 (-1.11)	
Si ML/LTO surface	$d_{1,2} (\delta_{1,2})$ La-top 1.83 (-0.33)	$d_{2,3} (\delta_{2,3})$ O-top 1.83 (-0.39)	$d_{3,4} (\delta_{3,4})$ 1.83 (-0.40)	$d_{4,5} (\delta_{4,5})$ 1.77 (-1.25)	$d_{5,6} (\delta_{5,6})$ 2.04 (2.42)	$d_{6,7} (\delta_{6,7})$ 1.80 (-0.74)	Δd 1.77 (-0.96)
Si ML/LLTO surface	Li-top 1.74 (-2.76)	O-top 1.75 (-2.66)	1.83 (0.41)	1.82 (0.36)	1.72 (-3.09)	2.30 (4.71)	2.30
Ge ML/LTO surface	La-top 1.83 (-0.35)	O-top 1.84 (-0.20)	1.83 (-0.43)	1.76 (-1.27)	2.03 (2.25)	1.80 (-0.78)	1.85 (-0.05)
Ge ML/LLTO surface	Li-top 1.72 (-2.97)	O-top 1.81 (-1.82)	1.84 (0.53)	1.94 (1.16)	2.03 (2.30)	1.87 (0.22)	1.78 (-1.02)
				1.81 (0.15)	1.70 (-3.29)	2.29 (4.59)	1.86 (-0.4)
				1.81 (0.19)	1.70 (-3.31)	2.29 (4.58)	2.06
						1.68 (-1.65)	1.98
						1.69 (-1.51)	1.94

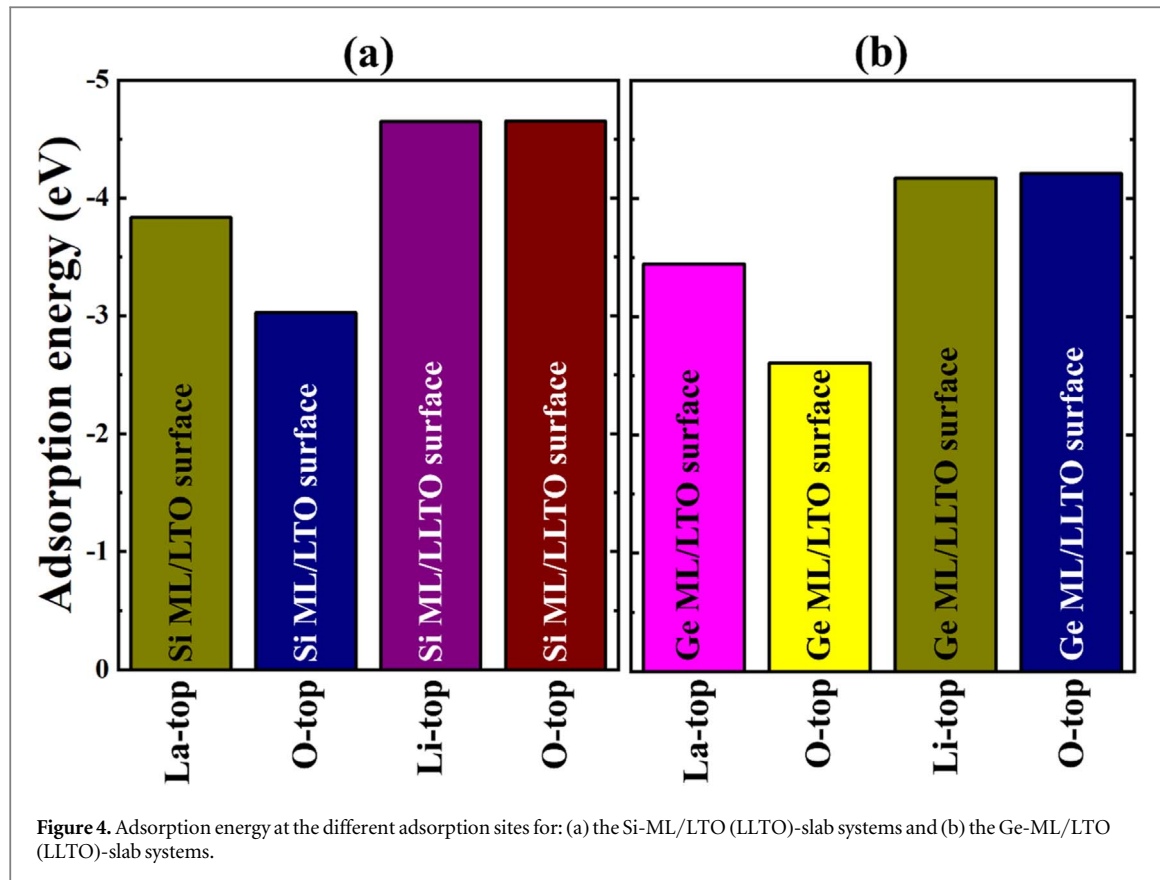


Figure 4. Adsorption energy at the different adsorption sites for: (a) the Si-ML/LTO (LLTO)-slab systems and (b) the Ge-ML/LTO (LLTO)-slab systems.

Table 4. Adsorption energy for the Si/Ge ML when it is adsorbed on the LTO or LLTO surfaces at different adsorption sites.

	Si ML/LTO surface		Si ML/LLTO surface		Ge ML/LTO surface		Ge ML/LLTO surface	
	La-top	O-top	Li-top	O-top	La-top	O-top	Li-top	O-top
E_{ads} (eV)	-3.83	-3.03	-4.65	-4.65	-3.45	-2.61	-4.17	-4.21

$d_{4,5}$ increases by 2.42%, while in the Ge ML case, it increases by 2.25%. When Si/Ge ML is adsorbed at the O-top site on the LaO-terminated LTO surface, $d_{1,2}$ and $d_{6,7}$ decrease, while the other interplanar distances increase. The largest increase is observed for $d_{4,5}$, with an increase of 2.32% for Si and 2.30% for Ge. In cases where Si/Ge ML was placed on the LiO-terminated LLTO surface, the Si/Ge ML stabilizes at the O-top sites, regardless of its initial position before structural relaxation. As a result, these semiconductor/oxide interfaces exhibit a consistent pattern in the change of interplanar distances: $d_{1,2}$, $d_{4,5}$, and $d_{6,7}$ decrease, while $d_{2,3}$, $d_{3,4}$, and $d_{5,6}$ increase.

On the other hand, the equilibrium distance (Δd) between the Si/Ge ML and the LaO-terminated LTO surface is larger compared to when the Si/Ge ML is placed on the LiO-terminated LLTO surface (table 3). This indicates that the Si/Ge ML adheres more strongly to the LLTO surface than to the LTO surface. To confirm this result, the adsorption energy was calculated. Figure 4 and table 4 display the adsorption energies (E_{ads}) per adsorbed atom for each Si (or Ge) ML/LTO (or LLTO) surface system, with the Si/Ge ML positioned at different adsorption sites. Because of the magnitude of adsorption energies, it is possible to talk about chemisorption in all the cases studied (figure 4 and table 4). For the relaxed La-top site, the Si/Ge-ML is formed by zigzag-shaped atomic chains, and it is more strongly adhered to the LaO-terminated LTO surface compared to the case where the Si/Ge-ML is adsorbed on the O-top site. Here, E_{ads} per atom adsorbed for the Si/Ge ML at the relaxed La-top and O-top adsorption sites on the LaO-terminated LTO surface are -3.83/-3.45 and -3.03/-2.61 eV, respectively. In cases where the Si/Ge ML is initially placed on the Li-top site, and after structural relaxation it is adsorbed on the O-top site on the LiO-terminated LLTO surface, the energy with which each of the Si/Ge atoms are adsorbed is -4.65/-4.17 eV. This result is very similar to the case where the Si/Ge ML is initially placed on the LiO-terminated LLTO surface at the O-top site, whose E_{ads} is -4.65/-4.21 eV (figure 4 and table 4).

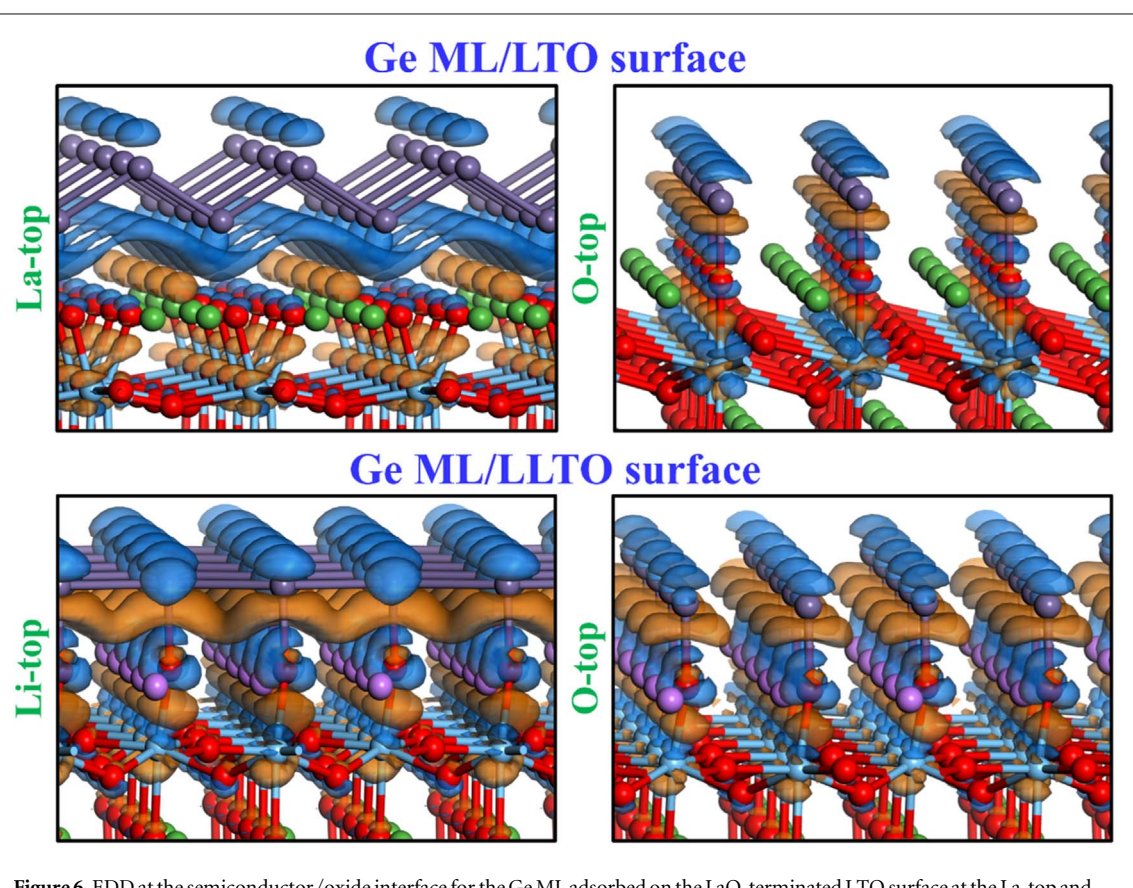
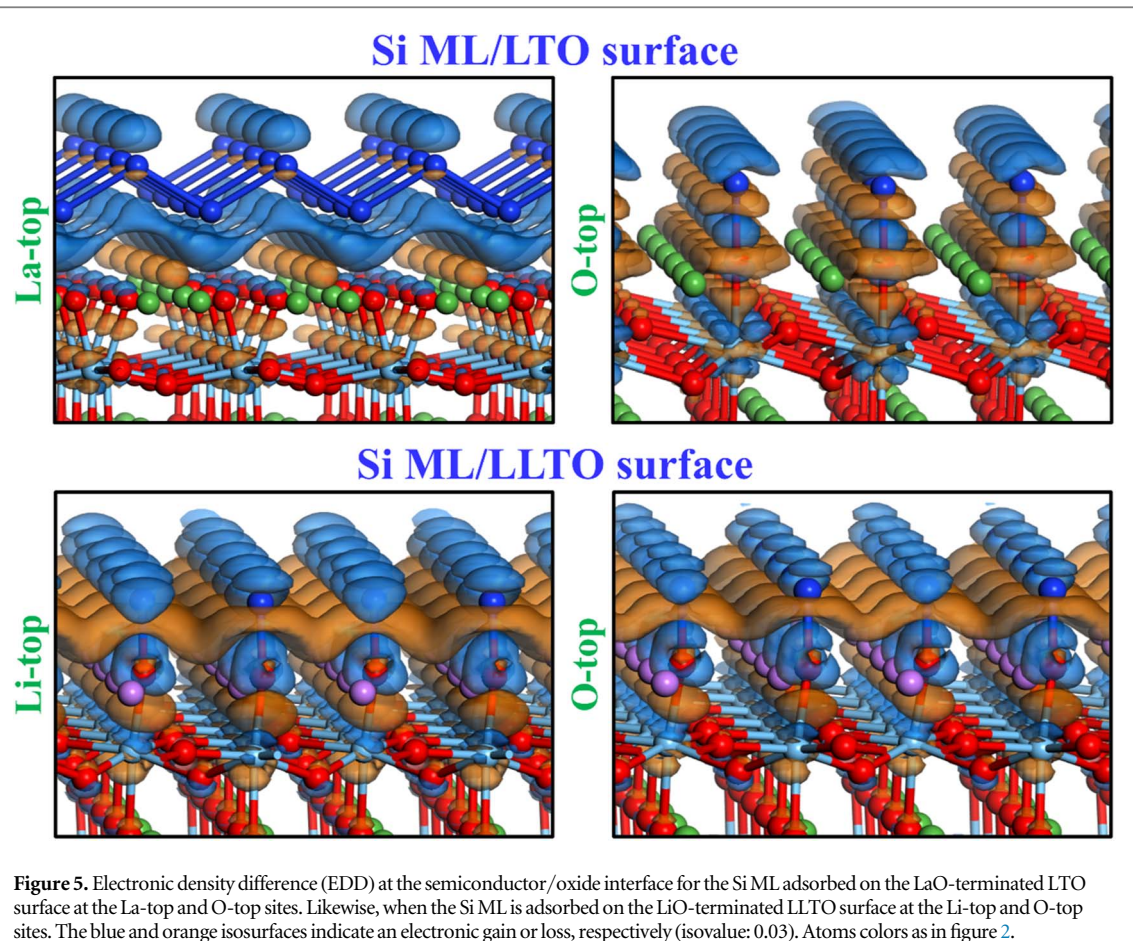


Table 5. Average atomic charge per layer (in e units) obtained through Hirshfeld analysis. There are atoms that have two different values of atomic charge. Due to the charges at each atomic site are significantly different and averaging them would not accurately reflect the electronic redistribution within these atoms.

		L ₁	L ₂	L ₃	L ₄	L ₅	L ₆	L ₇
LTO pristine surface		La	0.48		0.40		0.40	0.47
		Ti		0.40		0.48		0.40
		O	-0.37	-0.29	-0.28	-0.29	-0.29	-0.36
LLTO pristine surface		Li	0.30				0.18	
		La			0.37			0.56
		Ti		0.58		0.60		0.62
Si ML/LTO surface	La-top	O	-0.41	-0.30	-0.27	-0.30	-0.31	-0.41
		Si	-0.05					
		La	0.48, 0.34		0.41,		0.31	0.52
		Ti		0.43, 47		0.51,		0.38
		O	-0.34	-0.28	-0.29	-0.28	-0.28	-0.39
		Si	0.17					
		La	0.19		0.31		0.33	0.50
		Ti		0.35		0.57		0.35
		O	-0.29	-0.24	-0.30	-0.25	-0.30	-0.40
Si ML/LLTO surface	Li-top	Si	0.10					
		Li	0.15				0.18	
		La			0.36			0.56
		Ti		0.57		0.59		0.58
		O	-0.28	-0.31	-0.28	-0.30	-0.31	-0.40
		Si	0.11					
		Li	0.15				0.18	
		La			0.36			0.56
		Ti		0.57		0.58		0.59
Ge ML/LTO surface	La-top	O	-0.28	-0.31	-0.28	-0.30	-0.31	-0.31
		Ge	-0.02, -0.06					
		La	0.48, 0.33		0.41		0.30	0.52
		Ti		0.43, 0.47		0.50		0.38
		O	-0.34	-0.28	-0.29	-0.28	-0.28	-0.39
		Ge	0.17					
		La	0.20		0.31		0.33	0.49
		Ti		0.35		0.57		0.35
		O	-0.30	-0.24	-0.30	-0.25	-0.31	-0.40
Ge ML/LLTO surface	Li-top	Ge	0.11					
		Li	0.15				0.18	
		La			0.36			0.56
		Ti		0.57		0.59		0.58
		O	-0.29	-0.31	-0.28	-0.30	-0.31	-0.40
		Ge	0.10					
		Li	0.14				0.18	
		La			0.35			0.56
		Ti		0.58		0.59		0.58
		O	-0.29	-0.30	-0.28	-0.30	-0.31	-0.40

Thus, the most favorable place to put the Si/Ge ML on the LaO-terminated LTO surface is at the relaxed La-top adsorption site. In contrast, for systems where Si/Ge ML is adsorbed on the LiO-terminated LLTO surface, the most favorable site is the O-top. Besides, E_{ads} for cases where the Si/Ge ML is adsorbed on the LLTO surface is more negative compared to when it is adsorbed on the LTO surface. Consequently, Si/Ge ML is more strongly adhered to the LLTO surface. This finding agrees with the results obtained for Δd . An interesting observation is that the lowest E_{ads} occurs when the Si ML remains adhered to the O-top site on the LLTO surface, making it the most energetically stable configuration. In contrast, the highest E_{ads} is observed when the Ge ML adheres to the O-top site on the LTO surface; this E_{ads} is 43.87% higher than that of the Si ML on the LLTO surface at the O-top site. Finally, the Si ML remains more strongly adhered to than the Ge ML on the LTO and LLTO surfaces.

To investigate the adsorption mechanism of Si/Ge ML on LTO and LLTO surfaces, we analyzed the effects of Si/Ge adsorption on the electronic and magnetic properties of these semiconductor/oxide interfaces. This analysis involved calculating the electronic density difference (EDD), the partial density of states (PDOS) by spin channel, the distribution of magnetic moments, and the atomic orbitals through spin density at the E_F.

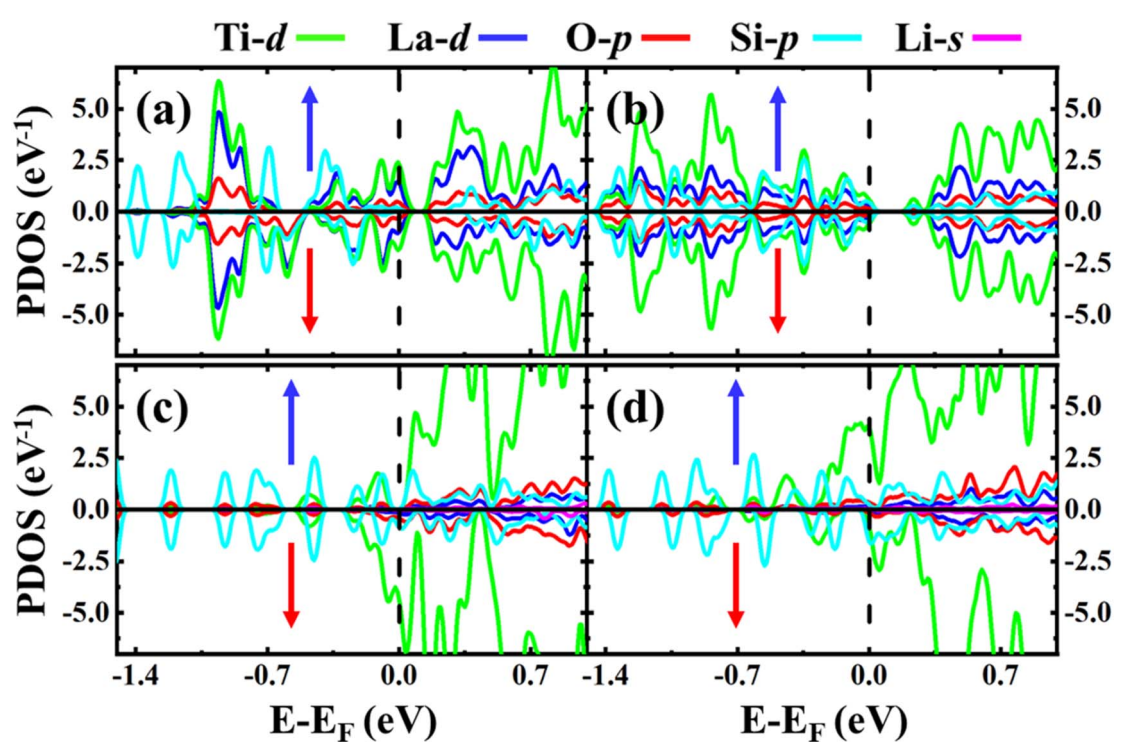


Figure 7. PDOS, by spin channel, when the Si-ML is adsorbed on LaO-terminated LTO surface with the ML at the La-top and O-top sites, (a) and (b), respectively; and the Si-ML adsorbed on LiO-terminated LLTO surface at the Li-top and O-top sites, (c) and (d), respectively. Black vertical dashed lines indicate the E_F. The up- and down-spin channels of PDOS are indicated by the blue and red arrows, respectively.

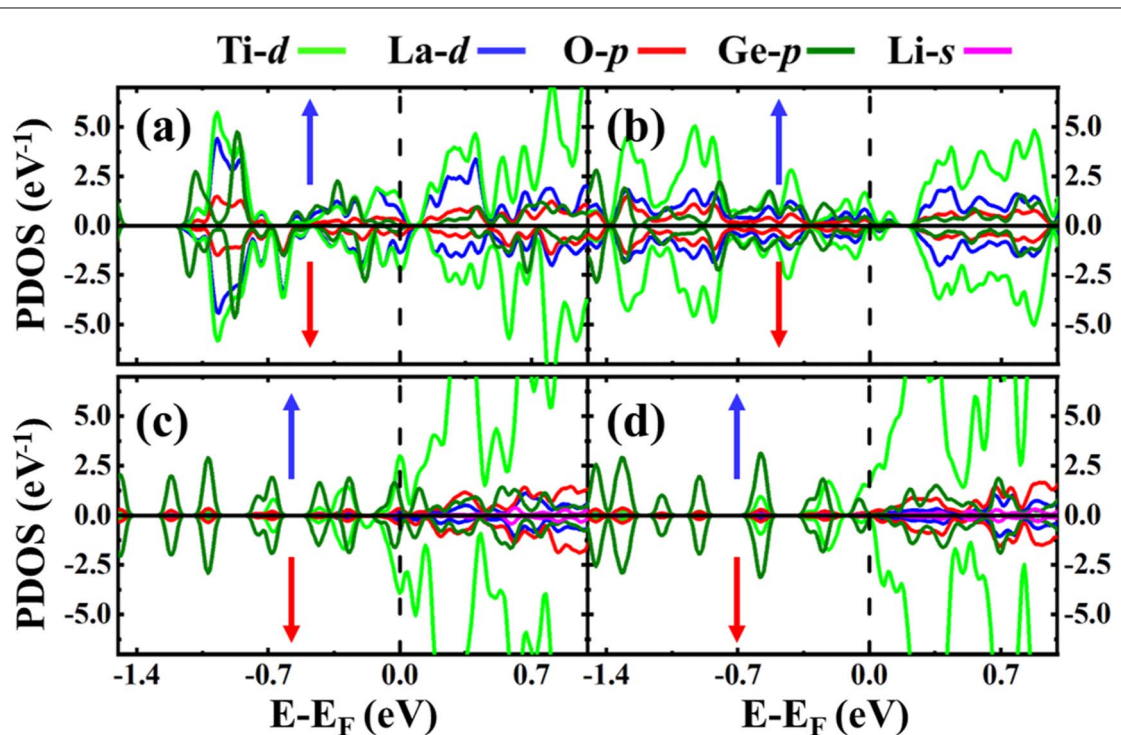
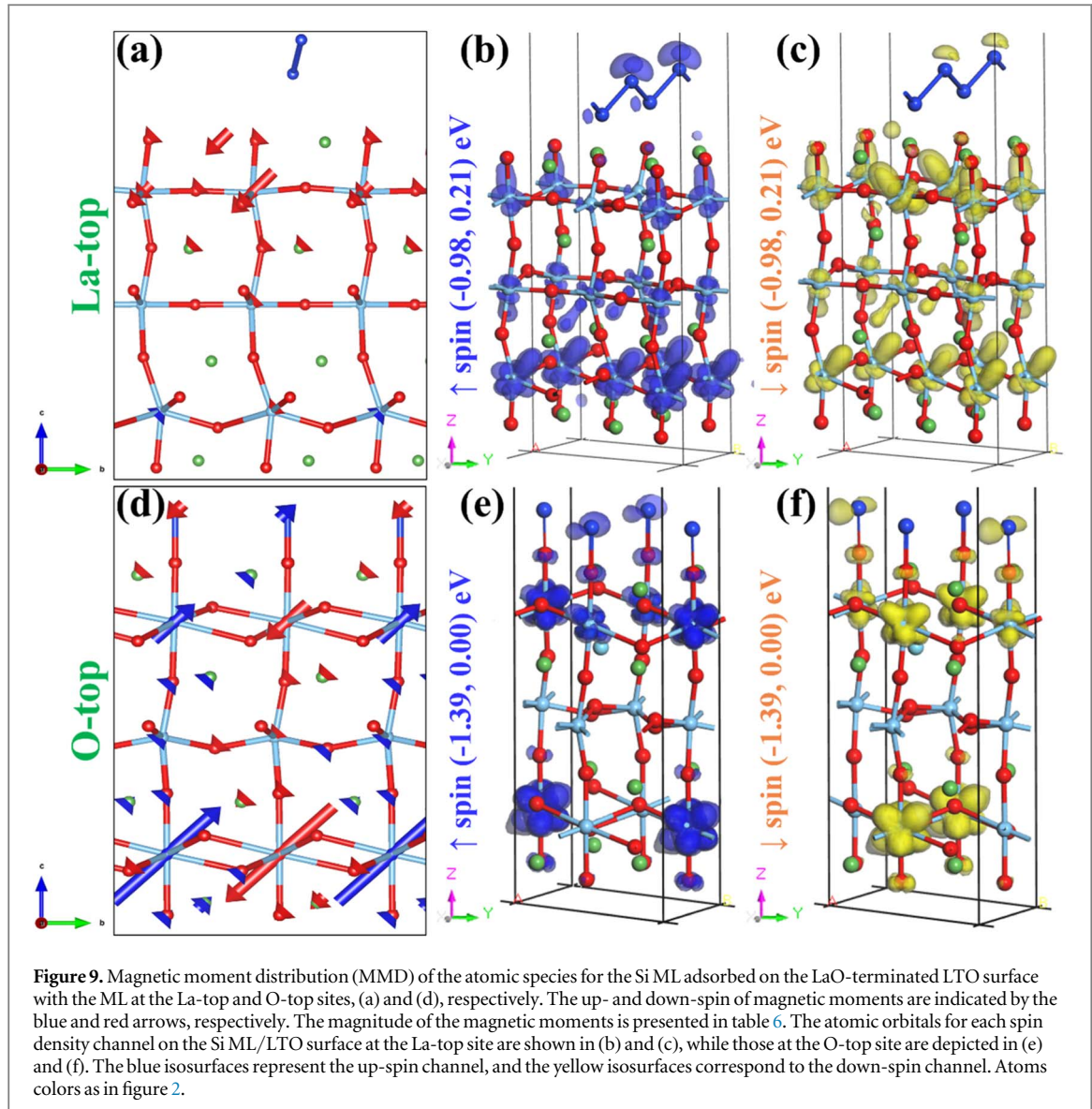


Figure 8. PDOS, by spin channel, when the Ge-ML is adsorbed on LaO-terminated LTO surface with the ML at the La-top and O-top sites, (a) and (b), respectively; and the Ge-ML adsorbed on LiO-terminated LLTO surface at the Li-top and O-top sites, (c) and (d), respectively. Black vertical dashed lines indicate the E_F. The up- and down-spin channels of PDOS are indicated by the blue and red arrows, respectively.

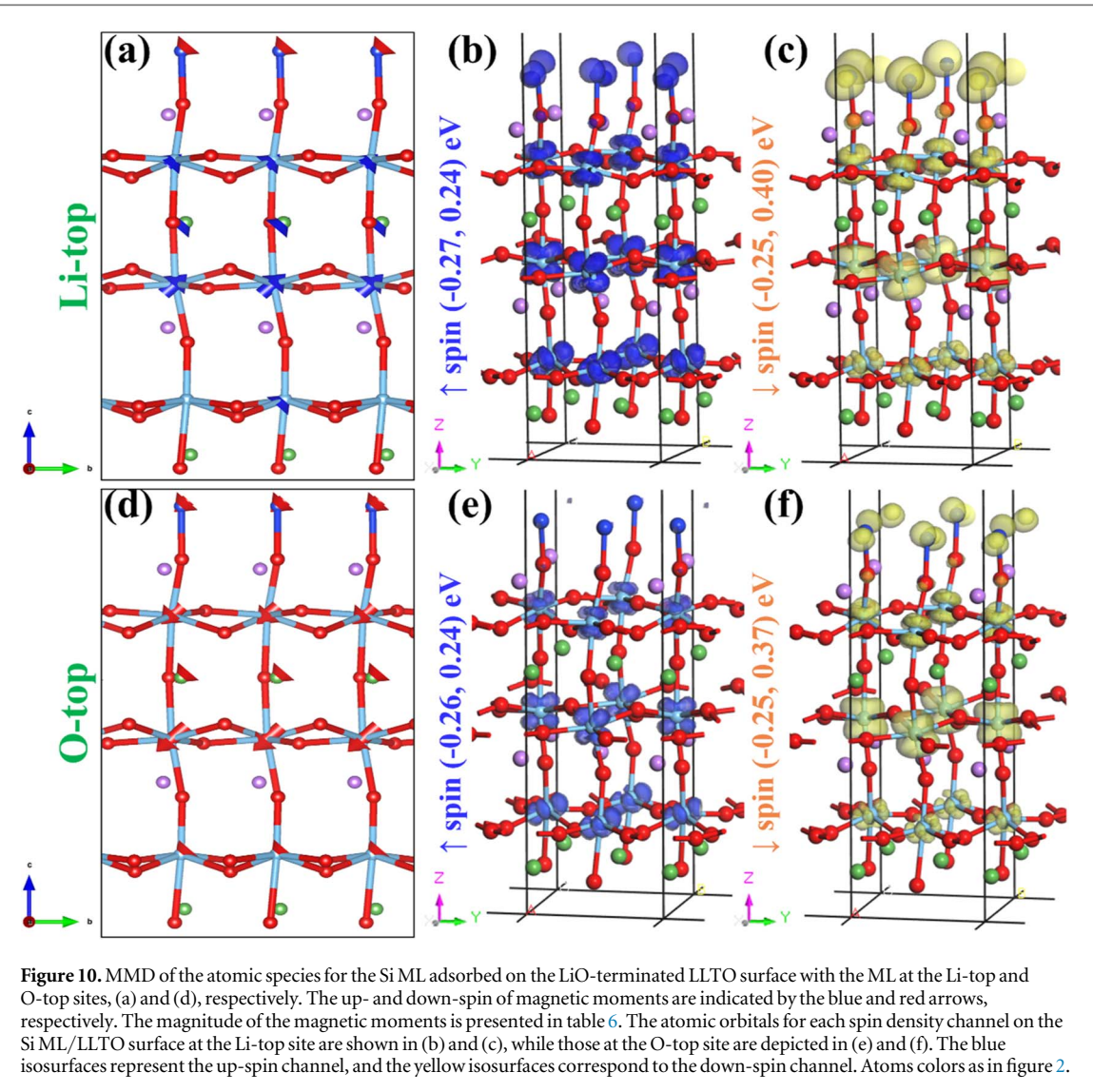


EDD at the semiconductor/oxide interface (SOI) for each studied system is shown in figures 5 and 6. For cases where the Si or Ge ML were placed at the La-top site on the LaO-terminated LTO surface, there are concentrations of electronic charge at the SOI. As can be seen in figures 5 and 6, it seems that the Ti and La atoms on the LTO surface are responsible for the electrons' contribution to the SOI, as there is a greater electronic loss on those atoms, compared to the regions of the electronic depletion for the Si or Ge ML. This charge redistribution can be understood through the electronegativities of Si, Ge, La, and Ti atoms, since the electronegativity of the Si/Ge, La and Ti atoms are very similar (on the Pauling scale, the Si/Ge, La and Ti atoms have an electronegativity of 1.90/2.00, 1.10 and 1.54, respectively) [70, 71]. Therefore, when these atoms interact, the electrons tend to be on the bond of a pair of interacting atoms instead of the atomic sites. This suggests that the interaction between the Si or Ge ML and the LaO-terminated LTO surface could be the covalent character.

In the Si (or Ge) ML/LTO surface cases, when the Si/Ge ML is adsorbed at the O-top site (figures 5 and 6), the electronic charge is located at the middle of the Si/Ge-O bonds, then these interactions could have a covalent character.

For the Si (or Ge) ML/LLTO surface cases, where the Si/Ge ML are at the O-top site, it was found that the O atoms gain electronic charge, and the Si/Ge atoms lose electrons. Thus, the Si or Ge ML is positively charged, while the LiO-terminated LLTO surface is negatively charged (figures 5 and 6). Therefore, the interaction between the Si or Ge ML and the LiO-terminated LLTO surface could be ionic.

Finally, for the Li-top adsorption site, after geometric optimization, the Si/Ge ML moves towards the O-top adsorption sites of the LiO-terminated LLTO surface. This position is similar to that observed for Si (or Ge) ML/LLTO surface at the O-top cases (figures 5 and 6). Thus, there exists an ionic interaction at the Si (or Ge)



ML/LLTO-slab systems at the SOI. It is worth mentioning that Si ML tends to transfer electrons more easily to their environment, compared to the Ge ML, for all systems, although Si and Ge have very similar electronegativities. This is evident as the electron depletion clouds surrounding the Si atoms are slightly larger than those observed for Ge (figures 5 and 6).

To quantify the observations from the EDD analysis, the average atomic charges per layer of SOI were obtained using Hirshfeld analysis. They were compared to those of the LTO and LLTO pristine surfaces (table 5). For the Si (or Ge)/LTO SOI at the La-top site, the La atoms in the first layer and Si atoms gain electronic charge, resulting in a decrease in their positive charge compared to the LTO pristine surface case. In contrast, the Ti atoms at the second layer loss electronic charge; Their atomic charge increases compared to the case of LTO pristine surface (table 5). For the case where the Si/Ge ML is adsorbed on the LaO-terminated LTO surface at the O-top site, the Si/Ge gains electronic charge ($\sim 0.17 e$). Specifically, the oxygen atoms in the first layer lose $\sim 0.07 e$, while the La atoms gain $\sim 0.28 e$. Additionally, in the second layer, the Ti atoms gain $\sim 0.05 e$ (table 5). Finally, when the Si/Ge ML interacts with the LiO-terminated LLTO surface, the charge redistribution behaves in the same way, regardless of where the Si/GeML was placed before structural relaxation. At the surface, the Si loses electronic charge ($0.11 e$), while the oxygen atoms transfer electronic charge to the Li atoms of the first ML (table 5). The redistribution of electronic charge supports the observations found in the EDD analysis.

Figures 7 and 8 show the partial density of the states (PDOS) by spin channel of the Si (or Ge) ML/LTO (or LLTO) surface system. In the case of the Si ML/LTO surface (La-top), PDOS displays an asymmetry between the electronic states of different spin channels within the energy range from -1.05 eV to E_F . This behavior indicates the presence of unpaired electrons, which contribute to the emergence of magnetic moments in the material. Furthermore, it can be observed that the electronic states cross the E_F , so the material is a conductor. The covalent character between the interaction of the Si ML and the LTO surface is observed, since the electronic

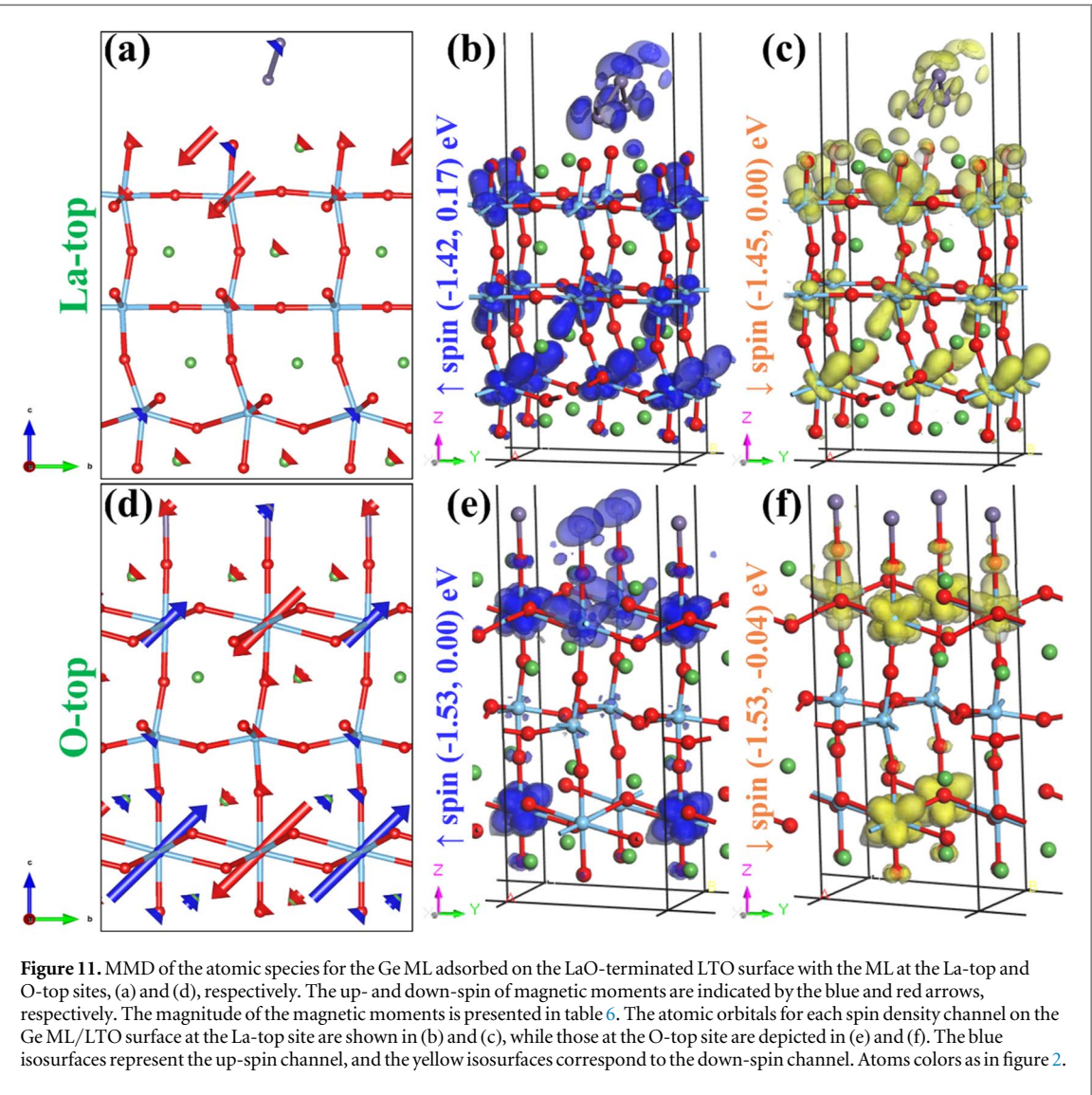


Figure 11. MMD of the atomic species for the Ge ML adsorbed on the LaO-terminated LTO surface with the ML at the La-top and O-top sites, (a) and (d), respectively. The up- and down-spin of magnetic moments are indicated by the blue and red arrows, respectively. The magnitude of the magnetic moments is presented in table 6. The atomic orbitals for each spin density channel on the Ge ML/LTO surface at the La-top site are shown in (b) and (c), while those at the O-top site are depicted in (e) and (f). The blue isosurfaces represent the up-spin channel, and the yellow isosurfaces correspond to the down-spin channel. Atoms colors as in figure 2.

states of the Si-*p* and O-*p* orbitals overlap in certain energy intervals. The greatest contribution to electronic states in the valence band (VB) at the E_F , comes from the La-*d* and Ti-*d* orbitals (figure 7(a)).

Si ML/LTO surface (O-top site) has a symmetrical PDOS, as will be explained later, this is because it exhibits antiferromagnetic behavior. This SOI system is conductor due to the electronic states crossing the E_F . In this region, the main contributions to the electronic states arise from the Si-*p* and Ti-*d* orbitals (figure 7(b)). For the cases where Si ML is placed on the LiO-terminated LLTO surface at the Li-top and O-top sites, the energy states of the unpaired electrons are in the energy range from -0.4 eV to E_F , the character of these electronic states is Si-*d* and Ti-*d* (figures 7(c) and (d)). Due to the presence of electronic states that intersect the E_F , these materials exhibit metallic properties.

PDOS for the Ge ML/LTO and Ge ML/LLTO surface systems at various adsorption sites is asymmetric, indicating that these materials exhibit magnetic properties. In all cases, the electronic states cross the E_F , confirming that they are conductors (figure 8). For the Ge ML/LTO system at the La-top site, the unpaired electrons are found within the energy range of -0.7 eV to E_F (figure 8(a)). For the case where GeML is at the O-top site on the LiO terminated LLTO surface, the electronic states of the unpaired electrons are in the energy range from -3.5 eV to E_F (figure 8(b)). Likewise, the electrons that induce magnetic moments in the GeML/LLTO surface systems at the La-top and O-top sites are found at energies from -1.75 eV to E_F (figures 8(c) and (d)).

For the cases shown in figures 8(a) and (b), the greatest contribution to electronic states at the E_F is provided by the Ge-*p*, La-*d* and Ti-*d* orbitals. In the Ge-ML/LLTO surface systems, where the Ge-ML is placed on the Li-top and O-top site, the main contribution to the electronic states at the E_F is supplied by the Ge-*p* and Ti-*d* orbitals (figures 8(c)–(d)).

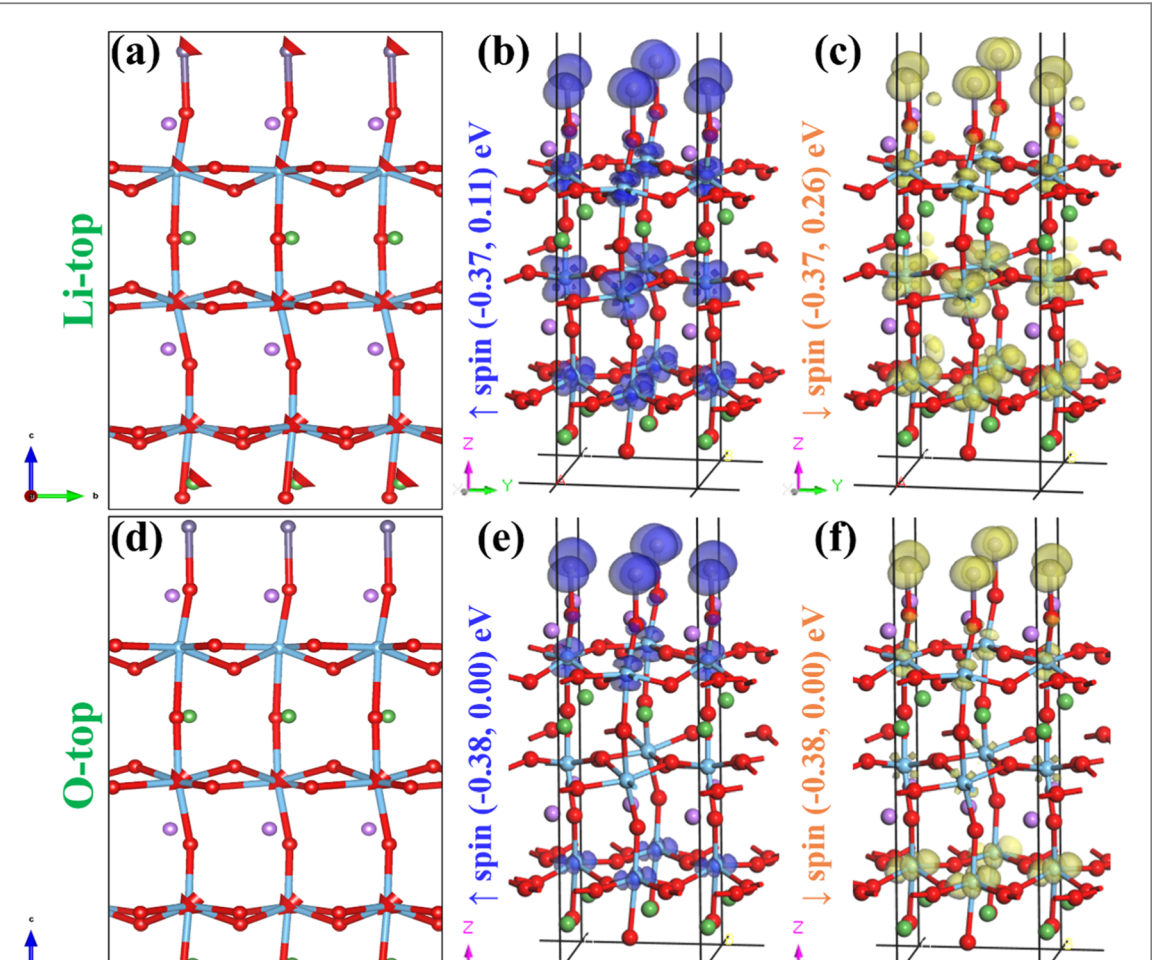


Figure 12. MMD of the atomic species for the Ge ML adsorbed on the LiO-terminated LLTO surface with the ML at the Li-top and O-top sites, (a) and (d), respectively. The up- and down-spin of magnetic moments are indicated by the blue and red arrows, respectively. The magnitude of the magnetic moments is presented in table 6. The atomic orbitals for each spin density channel on the Ge ML/LLTO surface at the Li-top site are shown in (b) and (c), while those at the O-top site are depicted in (e) and (f). The blue isosurfaces represent the up-spin channel, and the yellow isosurfaces correspond to the down-spin channel. Atoms colors as in figure 2.

To describe the magnetic configurations of SOI systems, we will use the following criteria: (i) If the distribution of magnetic moments shows pairs of electrons with antiparallel spins of the same magnitude, resulting in a total magnetic moment of zero, the material exhibits an antiferromagnetic configuration (AFM); (ii) If the magnetic moments of the atoms are parallel, regardless of whether they are of the same magnitude, the material is classified as ferromagnetic (FM). In this case, the total magnetic moment will be the sum of all individual moments; (iii) Finally, if the material has magnetic moments that are antiparallel with different magnitudes, and the total magnetic moment is not zero, it is categorized as ferrimagnetic. Consequently, to determine the magnetic configuration of SOI systems, we computed the distribution of magnetic moments for atomic species (figures 9–12). The magnitude of the magnetic moments is presented in table 6.

As mentioned earlier, when the Si-ML was placed at the La-top sites, the Si atoms moved away from the La atoms of the LaO-terminated LTO surface; here, the Si ML does not present magnetic moments. However, the Si ML indirectly affects the magnitude of the magnetic moments of the Ti atoms at the SOI, by means of a LaO ML, since the magnetic moments of the Ti atoms have a bigger magnitude when they are closer to the Si atoms, compared to the Ti atoms that are farther away. The material is ferrimagnetic (figure 9(a) and table 6). To understand the trends in the distribution of magnetic moments, the atomic orbitals by spin density were calculated. In figures 9(c) and (d), the spin-up and spin-down electron densities in layers 4 and 6 exhibit similar contributions from Ti-*d* states, resulting in small magnetic moments for the Ti atoms in these layers. In contrast, the Ti atoms in layer 2 show a greater contribution from the spin-down density, which leads to larger magnetic moments in the spin-down orientation for these atoms.

When Si-ML is adsorbed at the O-top site of the LaO-terminated LTO surface, the perovskite-type substrate generates magnetism to the Si atoms, resulting in an antiferromagnetic order of the system, whose magnitude of

Table 6. The moment magnitude (in μ_B) according to atom type and layer. In layers with AO stoichiometry (where A can be La or Li), there are two non-equivalent sites for metal A and two sites for oxygen atoms, resulting in two values for each atom type. Similarly, in layers with TiO_2 stoichiometry, there are two non-equivalent sites for Ti atoms and four for oxygen atoms, yielding two values for Ti and four values for oxygen. Additionally, the total magnetic moment (μ_T) is given for each case studied.

			L ₁	L ₂	L ₃	L ₄	L ₅	L ₆	L ₇	μ_T
Si ML/LTO surface	La-top	Si	0.00, 0.00							-1.03
		La	-0.22, -0.04		-0.02, -0.02		0.00, 0.00	0.01, -0.02	0.00, 0.00	
		Ti		-0.47, -0.11		-0.01, 0.00				
		O	-0.03, -0.02	-0.02, -0.03, 0.00, -0.01	-0.02, 0.00	0.00, 0.00, 0.00, 0.00	0.00, 0.00	0.00, 0.00, 0.00, 0.00	0.00, 0.00	
		Si	-0.09, 0.09				-0.03, 0.03			0.00
	O-top	La	-0.01, -0.01		-0.01, -0.01				-0.06, 0.06	
		Ti		-0.39, 0.39		-0.02, 0.02		-1.20, 1.20		
		O	0.00, 0.00	0.00, 0.00, 0.00, 0.00	-0.01, -0.01	-0.01, 0.01, 0.00, 0.00	-0.02, 0.02	-0.01, 0.01, 0.00, 0.00	-0.02, 0.02	
		Si	-0.01, -0.01							0.38
		Li	0.00, 0.00				0.00, 0.00			
Si ML/LLTO surface	Li-top	Si	-0.01, -0.01							
		La	0.00, 0.00		0.01, 0.01				0.00, 0.00	
		Ti		0.04, 0.04		0.14, 0.15		0.00, 0.01		
		O	0.00, 0.00	0.00, 0.00, 0.00, 0.00	0.00, 0.00	0.00, 0.00, 0.00, 0.00	0.00, 0.00	0.00, 0.00, 0.00, 0.00	0.00, 0.00	
		Si	-0.04, -0.04							-0.96
	O-top	Li	0.00, 0.00				0.00, 0.00			
		La			-0.02, -0.02				0.00, 0.00	
		Ti		-0.12, -0.12		-0.22, -0.20		-0.08, -0.10		
		O	0.00, 0.00	0.00, 0.00, 0.00, 0.00	0.00, 0.00	0.00, 0.00, 0.00, 0.00	0.00, 0.00	0.00, 0.00, 0.00, 0.00	0.00, 0.00	
		Si	-0.04, -0.04							
Ge ML/LTO surface	La-top	Ge	0.00, 0.01							-0.96
		La	-0.37, -0.02		-0.01, 0.00		0.00, 0.00	0.06, -0.01	0.02, -0.01	
		Ti		-0.52, -0.07		-0.02, 0.00		0.06, -0.01		
		O	0.01, -0.01	0.01, 0.01, 0.01, 0.00	0.00, 0.00	0.00, 0.00, 0.00, 0.00	0.00, 0.00	0.00, 0.00, 0.00, 0.00	0.00, 0.00	
		Si	-0.08, 0.06							-0.48
	O-top	Li	-0.04, -0.02		0.00, -0.04		-0.04, 0.04		-0.06, 0.06	
		Ti		0.48, -0.82		-0.02, 0.02		-1.20, 1.20		
		O	0.00, 0.00	0.00, 0.00, 0.00, 0.00	0.00, -0.02	0.00, 0.00, 0.00, 0.00	-0.02, 0.02	0.00, 0.00, 0.00, 0.00	-0.02, 0.02	
		Si	-0.02, -0.02							-0.52
		Ge	0.00, 0.00				0.00, 0.00			
Ge ML/LLTO surface	Li-top	Li	0.00, 0.00				0.00, 0.00			
		La			0.00, 0.00				-0.02, -0.02	
		Ti		-0.02, -0.02		-0.10, -0.10		-0.10, -0.10		
		O	0.00, 0.00	0.00, 0.00, 0.00, 0.00	0.00, 0.00	0.00, 0.00, 0.00, 0.00	0.00, 0.00	0.00, 0.00, 0.00, 0.00	0.00, 0.00	
		Si	-0.02, -0.02							-0.36
	O-top	Ge	0.00, 0.00							
		Li	0.00, 0.00				0.00, 0.00			
		La			0.00, 0.00				0.00, 0.00	
		Ti		0.00, 0.00		-0.08, -0.08		-0.10, -0.10		
		O	0.00, 0.00	0.00, 0.00, 0.00, 0.00	0.00, 0.00	0.00, 0.00, 0.00, 0.00	0.00, 0.00	0.00, 0.00, 0.00, 0.00	0.00, 0.00	

the magnetic moments increase in the Ti atoms at the layer 6 (figure 9(a) and table 6). These trends can be explained by the redistribution of electronic charge by spin. As can be seen in figures 9(e) and (f), the up- and down- spin densities are distributed along the Ti atoms in layer 2, so the magnitude of the magnetic moment is not as large as in the case of Ti atoms in layer 6, where the up-spin density is localized at one site of the Ti atom, while the down-spin density is localized at another site of the Ti atom.

For the Si ML/LLTO surface system, where the ML was placed at the Li-top site, the Si atoms did not remain above the Li atoms, they moved toward the O atoms closest to them and the magnitude of the magnetic moments of the Si atoms is $-0.01 \mu_B$. Ti atoms at the layer 4 of the LLTO surface present magnetic moments of greater magnitude compared to the Ti atoms of the other layers, and the magnetic moments have a ferrimagnetic order (figure 10(a) and table 6). When the Si ML is at the O-top site, the Si atoms practically do not move after the structural relaxation, this causes the distribution of magnetic moments adopting a ferromagnetic configuration (figure 10(b) and table 6). In these last two cases, the up- and down-spin densities are distributed almost equally over the atoms, resulting in a very small magnitude of magnetic moments (figures 10(b)–(c) and (e)–(f) and table 6).

When the Ge atoms are very far from the La atoms of the LTO surface, the Ge-ML has all its paired electrons, so, the magnetic moments of the Ge atoms are almost zero. As with Si, the magnitude of the magnetic moments of LTO surface are affected by Ge-ML; the material has a ferrimagnetic order (figure 11(a) and table 6).

When the Ge-ML is at the O-top site on the type-perovskite LTO surface, the Ge-ML is magnetic, and the Ge-ML/LTO-slab system has a ferrimagnetic order (figure 11(b) and table 6). Likewise, when the Ge ML is placed on LLTO surface at the Li-top and O-top adsorption sites, the distribution of magnetic moments exhibits ferromagnetic behavior (figure 12 and table 6).

Conclusions

In summary, we have studied the way to modulate the electronic and magnetic properties of the Si/Ge MLs on LTO/LLTO surface for semiconductor/oxide systems by means of DFT calculations using the Hubbard-corrected Local Density Approximation.

Structural results indicate that the interplanar distances decrease for the LTO pristine surface, whereas they increase for the LLTO pristine surface. Nonetheless, the interplanar distances are modified due to the effect of the absorption of the Si/Ge atoms modulating the surface properties.

Furthermore, the PDOS displays that all semiconductor/oxide interface systems are metallic. Additionally, the adsorption energy suggests that the most favorable site for placing Si ML is the O-top on the LiO-terminated LLTO surface.

When Si/Ge ML is initially placed at the La-top adsorption site on the LTO surface, the Si/Ge atoms move away from the La atoms on the LTO-slab surface. Here, the Si ML does not present magnetic moments, but it influences the ferrimagnetic ordering of the LTO surface. In the case where the Si/Ge ML are adsorbed at the O-top site on the LTO surface, the LTO surface induced magnetic moments on semiconductor atoms, and the system has an antiferromagnetic order.

These results indicate that the Si/Ge semiconductor ML/oxide perovskite surface can serve as an interface in electrochemical systems, as well as in devices that are magnetic, ferroelectric, or piezoelectric.

Acknowledgments

This work was partially supported by the projects DGAPA- UNAM IN103923 and IN100222, as well as IA103923. J M Cervantes acknowledges the postdoctoral scholarship granted by SECIHTI. J. E. Antonio and H. Muñoz acknowledge the postdoctoral scholarship granted by Dirección General de Asuntos del Personal Académico: Programa de Becas Posdoctorales en la UNAM. This work was supported by UNAM Postdoctoral Program (POSDOC). R. O. Escamilla wants to acknowledge support from SECIHTI and BEIFI-IPN. The authors thankfully acknowledge the computer resources, technical expertise and support provided by the Laboratorio Nacional de Supercálculo del Sureste de México, CONACYT member of the network of national laboratories. Calculations were done using resources from the Supercomputing Center DGTIC- UNAM.

Data availability statement

All data that support the findings of this study are included within the article (and any supplementary files).

ORCID iDs

- J M Cervantes  <https://orcid.org/0000-0003-3714-1774>
J E Antonio  <https://orcid.org/0000-0001-8136-3521>
H Muñoz  <https://orcid.org/0000-0001-8213-1466>
R O Escamilla  <https://orcid.org/0009-0000-1824-9275>
M Romero  <https://orcid.org/0000-0003-3363-757X>
R Escamilla  <https://orcid.org/0000-0002-6876-0351>

References

- [1] Hwang H Y, Iwasa Y, Kawasaki M, Keimer B, Nagaosa N and Tokura Y 2012 Emergent phenomena at oxide interfaces *Nat. Mater.* **11** 103–13
- [2] Droopad R, Contreras-Guerrero R, Veazey J P, Qiao Q, Klie R F and Levy J 2013 Epitaxial ferroelectric oxides on semiconductors- A route towards negative capacitance devices *Microelectron. Eng.* **109** 290–3
- [3] Chambers S A 2010 Epitaxial growth and properties of doped transition metal and complex oxide films *Adv. Mater.* **22** 219–48
- [4] Hong L, Bhatnagar K, Droopad R, Klie R F and Öğüt S 2017 Atomic-scale structural and electronic properties of SrTiO₃/GaAs interfaces: a combined STEM-EELS and first-principles study *Phys. Rev. B* **96**
- [5] Mazet L, Yang S M, Kalinin S V, Schamm-Chardon S and Dubourdieu C 2015 A review of molecular beam epitaxy of ferroelectric BaTiO₃ films on Si, Ge and GaAs substrates and their applications *Sci. Technol. Adv. Mater.* **16** 036005
- [6] Laughlin R P, Currie D A, Contreras-Guererro R, Dedigama A, Priyantha W, Droopad R, Theodoropoulou N, Gao P and Pan X 2013 17D919 [10.1063/1.4796150](https://doi.org/10.1063/1.4796150)
- [7] Dubourdieu C *et al* 2013 Switching of ferroelectric polarization in epitaxial BaTiO₃ films on silicon without a conducting bottom electrode *Nat. Nanotechnol.* **8** 748–54
- [8] Li Z, Guo X, Lu H B, Zhang Z, Song D, Cheng S, Bosman M, Zhu J, Dong Z and Zhu W 2014 An epitaxial ferroelectric tunnel junction on silicon *Adv. Mater.* **26** 7185–9
- [9] Zagidullina A E, Gumarova I I, Evseev A A and Mamin R F 2023 *Ab Initio* study of the electronic properties of a BaTiO₃/Si heterostructure *Bull. Russ. Acad. Sci. Phys.* **87** 488–91
- [10] Zheng N *et al* 2024 Perovskite-oxide-based ferroelectric synapses integrated on silicon *Adv. Funct. Mater.* **34** 1–9
- [11] Hu H *et al* 2024 Triple-junction perovskite-perovskite-silicon solar cells with power conversion efficiency of 24.4% *Energy Environ. Sci.* **17** 2800–14
- [12] Kumar A, Vandana, Dutta M, Srivastava S K and Pathi P 2024 Interface study of molybdenum oxide thin films on n- and p-type crystalline silicon surface *J. Mater. Sci., Mater. Electron.* **35** 1–13
- [13] Ngai J H, Kumah D P, Ahn C H and Walker F J 2014 Hysteretic electrical transport in BaTiO₃/Ba1–xSr_xTiO₃/Ge heterostructures *Appl. Phys. Lett.* **104** 062905
- [14] Ponath P *et al* 2015 Carrier density modulation in a germanium heterostructure by ferroelectric switching *Nat. Commun.* **6** 6067
- [15] Dogan M and Ismail-Beigi S 2017 *Ab initio* study of the BaTiO₃/Ge interface *Phys. Rev. B* **96** 1–14
- [16] Wang Z, Zhang Y, Chen H, He L, Jia Q, Liao M and Zhou Y 2025 Impact of La₂O₃ cap layer on 1/f noise in Ge-based nMOSFETs: insights from first-principles calculations *Physica B Condens Matter.* **700** 1–8
- [17] Kolpak A M *et al* 2010 Interface-induced polarization and inhibition of ferroelectricity in epitaxial SrTiO₃/Si *Phys. Rev. Lett.* **105** 1–4
- [18] Callori S J, Hu S, Bertinshaw J, Yue Z J, Danilkin S, Wang X L, Nagarajan V, Klose F, Seidel J and Ulrich C 2015 Strain-induced magnetic phase transition in SrCoO₃-δ thin films *Phys. Rev. B* **91** 1–5
- [19] Lee J H and Rabe K M 2011 Coupled magnetic-ferroelectric metal-insulator transition in epitaxially strained SrCoO₃ from first principles *Phys. Rev. Lett.* **107** 1–4
- [20] McDaniel M D, Ngo T Q, Hu S, Posadas A, Demkov A A and Ekerdt J G 2015 Atomic layer deposition of perovskite oxides and their epitaxial integration with Si, Ge, and other semiconductors *Appl. Phys. Rev.* **2** 1–32
- [21] Wagué B, Brubach J B, Niu G, Dong G, Dai L, Roy P, Saint-Girons G, Rojo-Romeo P, Robach Y and Vilquin B 2020 Structural studies of epitaxial BaTiO₃ thin film on silicon *Thin Solid Films* **693** 1–5
- [22] Wen Y, Chen H, Wu Z, Li W and Zhang Y 2024 Fabrication and photonic applications of Si-integrated LiNbO₃ and BaTiO₃ ferroelectric thin films *APL Mater.* **12** 1–29
- [23] Abel S *et al* 2013 A strong electro-optically active lead-free ferroelectric integrated on silicon *Nat. Commun.* **4** 1
- [24] Haque A, D’Souza H J, Parate S K, Sandilya R S, Raghavan S and Nukala P 2024 Heterogeneous integration of high endurance ferroelectric and piezoelectric epitaxial BaTiO₃ devices on Si *Adv. Funct. Mater.* **35** 1–10
- [25] Tao M, Zhang B, Zhao T, Wu X, Liu M, Dong G and Wang J 2024 Towards high quality transferred barium titanate ferroelectric hybrid integrated modulator on silicon *Light: Advanced Manufacturing* **5** 1–11
- [26] Jin E N, Kornblum L, Kumah D P, Zou K, Broadbridge C C, Ngai J H, Ahn C H and Walker F J 2014 A high density two-dimensional electron gas in an oxide heterostructure on Si (001) *APL Mater.* **2** 116109–1
- [27] Biscaras J, Bergeal N, Hurand S, Grosssetete C, Rastogi A, Budhani R C, LeBoeuf D, Proust C and Lesueur J 2012 Two-dimensional superconducting phase in LaTiO₃/SrTiO₃ heterostructures induced by high-mobility carrier doping *Phys. Rev. Lett.* **108** 247004–1
- [28] Jahangir-Moghadam M, Ahmadi-Majlan K, Shen X, Droubay T, Bowden M, Chrysler M, Su D, Chambers S A and Ngai J H 2015 Band-gap engineering at a semiconductor-crystalline oxide interface *Adv. Mater. Interfaces* **2** 1400497
- [29] Baldini M, Muramatsu T, Sherafati M, Mao H K, Malavasi L, Postorino P, Satpathy S and Struzhkin V V 2015 Origin of colossal magnetoresistance in LaMnO₃ manganite *Proc. Natl. Acad. Sci. U.S.A.* **112** 10869–72
- [30] Kumah D P, Ngai J H and Kornblum L 2020 Epitaxial oxides on semiconductors: from fundamentals to new devices *Adv. Funct. Mater.* **30** 1–37
- [31] Sun Y, Guan P, Liu Y, Xu H, Li S and Chu D 2019 Recent progress in lithium lanthanum titanate electrolyte towards all solid-state lithium ion secondary battery *Crit. Rev. Solid State Mater. Sci.* **44** 265–82
- [32] Wu J, Chen L, Song T, Zou Z, Gao J, Zhang W and Shi S 2017 A review on structural characteristics, lithium ion diffusion behavior and temperature dependence of conductivity in perovskite-type solid electrolyte Li_{3x}La_{2/3-x}TiO₃ *Functional Materials Letters* **10** 1–11

- [33] Bachman J C *et al* 2016 Inorganic solid-state electrolytes for lithium batteries: mechanisms and properties governing ion conduction *Chem. Rev.* **116** 140–62
- [34] Aaltonen T, Alnes M, Nilsen O, Costelle L and Fjellvåg H 2010 Lanthanum titanate and lithium lanthanum titanate thin films grown by atomic layer deposition *J. Mater. Chem.* **20** 2877–81
- [35] Gobaut B, Penuelas J, Benamrouche A, Robach Y, Blanc N, Favre-Nicolin V, Renaud G, Largeau L and Saint-Girons G 2014 Growth of Ge islands on SrTiO₃ (001) 2 × 1 reconstructed surface: epitaxial relationship and effect of the temperature *Surf. Sci.* **624** 130–4
- [36] Deng W, Yang M, Chai J, Wong T I, Du A, Ng C M, Feng Y and Wang S 2012 Orientation control of epitaxial Ge thin films growth on SrTiO₃ (100) by ultrahigh vacuum sputtering *Thin Solid Films* **520** 4880–3
- [37] Danescu A, Penuelas J, Gobaut B and Saint-Girons G 2016 Texture of Ge on SrTiO₃ (001) substrates: evidence for in-plane axiotaxy *Surf. Sci.* **644** 13–7
- [38] Zanouni M, Denys E, Derivaz M, Dentel D, Diani M, Azzouz C B and Bischoff J L 2014 Growth of Fe nanocrystals on LaAlO₃ (001) and epitaxial relationship determination by RHEED and XPS *Physica Status Solidi (C) Current Topics in Solid State Physics* **11** 1393–6
- [39] Wang J and Lefebvre I 2012 Germanium adsorption on SrTiO₃ (001) 2 × 1 surface: a density functional theory study *Adv Mat Res* **463–464** 484–8
- [40] Wang J and Lefebvre I 2013 Germanium growth orientation on SrTiO₃ (001) 2 × 1 surface: role of surface reduction *J. Phys. Chem. C* **117** 9887–94
- [41] Wang J, Wang C, Tang G, Zhang J, Guo S and Han Y 2016 Interface properties of Ge on cubic SrHfO₃ (001) *J. Cryst. Growth* **443** 66–74
- [42] Wang C, Wang J, Yuan M, Zhang J, Tang G, Han Y and Wu X S 2016 The structure and electronic properties of Ge/SrZrO₃ *Vacuum* **130** 165–73
- [43] Clark S J, Segall M D, Pickard C J, Hasnip P J, Probert M I J, Refson K and Payne M C 2005 First principles methods using CASTEP *Z Kristallogr Cryst. Mater.* **220** 567–70
- [44] BIOVIA 2018 Castep guide materials studio 2019 *Dassault Systèmes*
- [45] Anisimov V I, Zaanen J and Andersen O K 1991 Band theory and Mott insulators: Hubbard U instead of Stoner *I Phys. Rev. B* **44** 943–54
- [46] Ceperley D M and Alder B J 1980 Ground state of the electron gas by a stochastic method *Phys. Rev. Lett.* **45** 566–9
- [47] Perdew J P and Zunger A 1981 Self-interaction correction to density-functional approximations for many-electron systems *Phys. Rev. B* **23** 5048–79
- [48] Streltsov S V, Mylnikova A S, Shorikov A O, Pchelkina Z V, Khomskii D I and Anisimov V I 2005 Crystal-field splitting for low symmetry systems in *ab initio* calculations *Phys. Rev. B Condens. Matter Mater. Phys.* **71** 1–13
- [49] Monkhorst H J and Pack J D 1976 Special points for Brillouin-zone integrations *Phys. Rev. B* **13** 5188–92
- [50] Barzilai J and Borwein J M 1988 Two-point step size gradient methods *IMA J. Numer. Anal.* **8** 141–8
- [51] Komarek A C, Roth H, Cwik M, Stein W-D, Baier J, Kriener M, Bourée F, Lorenz T and Braden M 2007 Magnetoelastic coupling in RTiO₃ (R=La, Nd, Sm, Gd, Y) investigated with diffraction techniques and thermal expansion measurements *Phys. Rev. B* **75** 224402–1
- [52] Wu H, Aoki T, Posadas A B, Demkov A A and Smith D J 2016 Anti-phase boundaries at the SrTiO₃/Si(001) interface studied using aberration-corrected scanning transmission electron microscopy *Appl. Phys. Lett.* **108** 1–5
- [53] Demkov A A, Ponath P, Fredrickson K, Posadas A B, McDaniel M D, Ngo T Q and Ekerdt J G 2015 Integrated films of transition metal oxides for information technology *Microelectron. Eng.* **147** 285–9
- [54] Eglitis R I and Popov A I 2018 Systematic trends in (001) surface *ab initio* calculations of ABO₃ perovskites *Journal of Saudi Chemical Society* **22** 459–68
- [55] Cervantes J M, Pilo J, Rosas-Huerta J L, Antonio J E, Muñoz H, Oviedo-Roa R and Carvajal E 2021 DFT electronic properties and synthesis thermodynamics of Li_xLa_{1-x}TiO₃ electrolytes for Li-Ion batteries *J. Electrochem. Soc.* **168** 080516
- [56] Cervantes J M, Antonio J E, Rosas-Huerta J L, Muñoz H, Pilo J, Carvajal E, Arévalo-López E P, Romero M and Escamilla R 2023 Effects of high hydrostatic pressure on the structural, electronic, and elastic properties, and li-ion diffusion barrier of lithium lanthanum titanate electrolytes: A DFT study *J. Electrochem. Soc.* **170** 110528
- [57] An M, Zhang H-M, Weng Y-K, Zhang Y and Dong S 2016 Possible ferrimagnetism and ferroelectricity of half-substituted rare-earth titanate: a first-principles study on Y0.5La0.5TiO₃ *Front Phys. (Beijing)* **11** 117501
- [58] Antonio J E, Rosas-Huerta J L, Cervantes J M, León-Flores J, Romero M, Carvajal E and Escamilla R 2023 Li/Na atoms' substitution effects on the structural, electronic, and mechanical properties of the CaSnO₃ perovskite for battery applications *Comput. Mater. Sci.* **219** 112006
- [59] Antonio J E, Cervantes J M, Muñoz H, Arévalo-López E P, Romero M, Carvajal E and Escamilla R 2024 Substitution effects on the structural, mechanical, electronic and electrochemical properties of lithium/sodium strontium stannate perovskite for battery applications *J. Phys. Chem. Solids* **189** 111935
- [60] Cheng Y Q, Bi Z H, Huq A, Feygenson M, Bridges C A, Paranthaman M P and Sumpter B G 2014 An integrated approach for structural characterization of complex solid state electrolytes: The case of lithium lanthanum titanate *J. Mater. Chem. A Mater.* **2** 2418–26
- [61] Moriwake H, Gao X, Kuwabara A, Fisher C A J, Kimura T, Ikuhara Y H, Kohama K, Tojigamori T and Ikuhara Y 2015 Domain boundaries and their influence on Li migration in solid-state electrolyte (La,Li)TiO₃ *J. Power Sources* **276** 203–7
- [62] Antonio J E, Cervantes J M, Rosas-Huerta J L, Romero M, Escamilla R and Carvajal E 2021 Exposed surface and confinement effects on the electronic, magnetic, and mechanical properties of LaTiO₃ slabs *IEEE Trans. Magn.* **57** 1–4
- [63] Ortmann F, Bechstedt F and Schmidt W G 2006 Semiempirical van der Waals correction to the density functional description of solids and molecular structures *Phys. Rev. B* **73** 205101
- [64] Okimoto Y, Katsufuji T, Okada Y, Arima T and Tokura Y 1995 Optical spectra in (La,Y)TiO₃: variation of mott-hubbard gap features with change of electron correlation and band filling *Phys. Rev. B* **51**
- [65] Cwik M *et al* 2003 Crystal and magnetic structure of LaTiO₃ Evidence for nondegenerate t_{2g} orbitals *Phys. Rev. B* **68** 060401
- [66] Goral J P and Greeden J E 1983 The magnetic structures of LaTiO₃ and CeTiO₃ *J. Magn. Magn. Mater.* **37** 315–21
- [67] El-Mellouhi F, Brothers E N, Lucero M J, Bulik I W and Scuseria G E 2013 Structural phase transitions of the metal oxide perovskites SrTiO₃, LaAlO₃, and LaTiO₃ studied with a screened hybrid functional *Phys. Rev. B* **87** 035107
- [68] Gu M and Rondinelli J M 2016 Ultrafast band engineering and transient spin currents in antiferromagnetic oxides *Sci. Rep.* **6** 1–10
- [69] Filippetti A, Pemmaraju C D, Sanvito S, Delugas P, Puggioni D and Fiorentini V 2011 Variational pseudo-self-interaction-corrected density functional approach to the *ab initio* description of correlated solids and molecules *Phys. Rev. B Condens. Matter Mater. Phys.* **84** 195127
- [70] Smith D W 2007 A new approach to the relationship between bond energy and electronegativity *Polyhedron* **26** 519–23
- [71] Ohwada K 1984 On the pauling electronegativity scales—II *Polyhedron* **3** 853–9